

G protein-specific mechanisms in the serotonin 5-HT_{2A} receptor regulate psychosis-related effects and memory deficits

Received: 23 June 2023

Accepted: 23 April 2024

Published online: 29 May 2024

 Check for updates

Elk Kossatz^{1,14}, Rebeca Diez-Alarcia^{2,3,4,14}, Supriya A. Gaitonde⁵, Carla Ramon-Duaso⁶, Tomasz Maciej Stepniowski^{7,8}, David Aranda-Garcia^{7,9}, Itziar Muneta-Arrate^{2,3}, Elodie Tepaz⁵, Suwipa Saen-Oon¹⁰, Robert Soliva¹⁰, Aida Shahraki¹¹, David Moreira^{12,13}, Jose Brea^{11,12}, Maria Isabel Loza^{12,13}, Rafael de la Torre¹, Peter Kolb¹¹, Michel Bouvier⁵, J. Javier Meana^{2,3,4}, Patricia Robledo¹✉ & Jana Selent^{7,9}✉

G protein-coupled receptors (GPCRs) are sophisticated signaling machines able to simultaneously elicit multiple intracellular signaling pathways upon activation. Complete (in)activation of all pathways can be counterproductive for specific therapeutic applications. This is the case for the serotonin 2A receptor (5-HT_{2A}R), a prominent target for the treatment of schizophrenia. In this study, we elucidate the complex 5-HT_{2A}R coupling signature in response to different signaling probes, and its physiological consequences by combining computational modeling, in vitro and in vivo experiments with human postmortem brain studies. We show how chemical modification of the endogenous agonist serotonin dramatically impacts the G protein coupling profile of the 5-HT_{2A}R and the associated behavioral responses. Importantly, among these responses, we demonstrate that memory deficits are regulated by G_{αq} protein activation, whereas psychosis-related behavior is modulated through G_{αi1} stimulation. These findings emphasize the complexity of GPCR pharmacology and physiology and open the path to designing improved therapeutics for the treatment of schizophrenia.

G protein-coupled receptors (GPCRs) are an important class of cell surface receptors. Due to their involvement in numerous physiological processes, they have become an important drug target class for numerous clinical indications, with 30-40% of marketed drugs acting through them¹. However, the signaling complexity of GPCRs related to their ability to signal through numerous pathways, including disease-associated but also non-disease-associated pathways, have been linked to undesired side effects². Moreover, the discovery that molecular modulators (so-called biased (ant)agonists) can bind to

GPCRs and preferentially activate specific pathways over others (so-called pathway bias) has created the opportunity to improve drug development for complex diseases such as schizophrenia (SCZ)³. SCZ is a severe debilitating disease, characterized by positive symptoms (such as hallucinations), negative symptoms (including amotivation, anhedonia and alogia), and cognitive deficits⁴. Current antipsychotic medications, however, do not target cognitive or negative symptoms, which are the main factors contributing to the loss of functionality in SCZ patients⁵. In addition, most of the patients that

A full list of affiliations appears at the end of the paper. ✉ e-mail: probledo@imim.es; jana.selent@upf.edu

receive antipsychotic treatment suffer diverse side effects, and up to 30% of patients are resistant or respond only partially to treatment⁶. Therefore, there is a clear need for improving treatment strategies. Classical and atypical antipsychotic drugs have traditionally been designed to inhibit implicated GPCRs without considering the different intracellular signaling pathways triggered by the receptors. Such non-selective inhibition of all possible pathways associated with one GPCR target can result in reduced therapeutic efficacy and provoke unwanted side effects⁷. This seems to be the case for the serotonin (5-HT) 2A receptor (5-HT_{2A}R)⁸, a prominent target for the treatment of SCZ. Recent studies have shown that inhibition of 5-HT_{2A}R-mediated pathways by antipsychotic drugs results in an unwanted silencing of the metabotropic glutamate receptor 2 (mGlu₂R) transcription, suggesting that full receptor inactivation could be counterproductive for the treatment of SCZ⁸. Hence, selectively modulating only pathway(s) linked to the disease is a promising approach to obtaining more efficacious and safer drugs. However, the contribution of specific 5-HT_{2A}R-initiated pathways to SCZ-like symptoms (i.e. positive, negative and cognitive deficits) via the engagement of various subtypes of G_α protein subunits, i.e. G_{αq} or G_{αi} proteins, and β-arrestins^{3,9–12} has remained largely elusive.

In this study, we successfully address the challenges of disentangling the role of 5-HT_{2A}R-mediated pathways in SCZ-like behavioral responses by applying a multidisciplinary approach. Using small molecular probes derived from the natural agonist 5-HT, we first reveal the complex 5-HT_{2A}R coupling signature across its different downstream transducers (G_{αq}, G_{αi}, β-arrestins 1 and 2) using live-cell bioluminescence resonance energy transfer (BRET)-based biosensors. Then, linking postmortem brain experiments with *in vivo* behavioral responses, we provide evidence that distinct 5-HT_{2A}R-mediated pathways are implicated in psychosis-related effects and memory deficits. These findings have been validated with pharmacological and genetic tools to determine G protein implication. Finally, molecular modeling and dynamics simulation of the binding of signaling probes with differential behavioral responses highlight the structural features underlying the different actions of 5-HT_{2A}R. Importantly, our findings have key implications for exploiting G protein-specific mechanisms not only for the design of a novel class of drugs with improved therapeutic profiles for the treatment of SCZ, but can also contribute to a better understanding of the disease etiology.

Results

BRET experiments reveal the complex spectrum of 5-HT_{2A}R signaling in living cells

To gain insight into the molecular determinants that drive ligand-mediated 5-HT_{2A}R signaling bias, we studied the engagement of the receptor's proximal effectors (G proteins and β-arrestins) upon stimulation with structurally closely related probes of the endogenous agonist 5-HT (Fig. 1), including Met-I (3-(2-aminoethyl)-1-methyl-1H-indol-5-yl hydrochloride), Nitro-I (2-(5-nitro-1H-indol-3-yl)ethamine hydrochloride), OTV1 (2-[5-(2,3-dihydro-1,4-benzodioxin-6-yl)-1H-indol-3-yl]ethan-1-amine) and OTV2 (2-(5-phenoxy-1H-indol-3-yl)ethan-1-amine)). The two latter compounds have been obtained from a virtual screen (see method section). Competition binding experiments

with [³H]-ketanserin confirm that the test compounds bind to the orthosteric binding site of the 5-HT_{2A}R (Fig. 1).

In a first screen, we explored the coupling spectrum of the 5-HT_{2A}R to several G_α protein subtypes and β-arrestins upon stimulation with Nitro-I, Met-I, OTV1 and OTV2 in living HEK-293 cells using BRET-based assays (Fig. 2A). The pEC₅₀, E_{max} and log τ/K_A for G_{αq}, G_{αi1}, G_{αi2}, G_{αi3}, G_{αoA}, G_{αoB}, and G_{αz} are listed in Table 1, whereas full concentration response curves are shown only for representative members of the G_{αq} and G_{αi} family and β-arrestin 1 and 2 in Fig. 2B–G. We find that all compounds are full agonists toward the canonical G_{αq} pathway, but only partial agonists on the G_{αi} family and βarrs when compared to 5-HT. Notably, among the G_{αi} family members, the relative efficacy is greater toward G_{αi1} vs G_{αi2}, or G_{αi3}. To further characterize the signaling profiles promoted by the 5-HT analogs, the transduction coefficient (log τ/K_A) was determined for each pathway using the operational model^{13,14} followed by calculation of the ligand-physiology bias⁷ factor between pathways using the endogenous agonist 5-HT as the reference.

Figure 2H illustrates the coupling preference and physiology-bias profile promoted by each of the compounds as compared to 5-HT. Nitro-I and Met-I show a general physiology bias for the canonical G_{αq} over G_{αi1}, G_{αi2}, G_{αi3}, β-arrestin 1, and 2 (light to dark blue, Fig. 2H). Of note is the high magnitude of G_{αq} bias over β-arrestin 2 for both compounds with 10 (Nitro-I) and > 50 fold (Met-I), and the high G_{αq} bias over G_{αi1} with > 50 (Nitro-I) and 8-fold bias (Met-I).

Interestingly, introducing an extended substituent (i.e. phenoxy substituent) in position 5 of the indole fragment (Fig. 1), as in OTV2, results in a distinct coupling (Fig. 2B–G) and bias profile of 5-HT_{2A}R (Fig. 2H) compared to Nitro-I and Met-I. OTV2 induces a general bias toward the G_{αi} family (G_{αi1}, G_{αi2}, G_{αi3}) over G_{αq} (light to dark red colors, Fig. 2H) in comparison to 5-HT, which is mainly driven by the increased potency of OTV2 towards the G_{αi} family members. Furthermore, we observe that OTV2 has a substantially reduced ability to promote the recruitment of β-arrestin 1, yielding a 17-fold G_{αq} bias over β-arrestin 1 while the G_{αq} bias over β-arrestin 2 observed for Nitro-I and Met-I was lost for OTV2 (Fig. 2H and Table 1).

Further extension of position 5 (i.e. 1,4-benzodioxin) (Fig. 1) produces the most dramatic changes in the coupling (Fig. 2B–G) and physiology-bias profile (Fig. 2H). OTV1 loses to a large extent its stimulating activity for G_{αi2}, G_{αi3} as well as its ability to recruit β-arrestin 1 and 2 (Fig. 2D–G). This results in a very significant G_{αq} activation preference over G_{αi1}, with a bias factor > 20 compared to 5-HT. An even greater preference is observed toward G_{αq} vs G_{αi2}, G_{αi3}, β-arrestin 1 and 2. However, virtually no activation of these pathways prevented us from calculating a formal bias factor (gray colored, Fig. 2H). Whether this preference results from a structurally-driven signaling bias or from the lower potency of OTV1 toward all pathways (i.e. activation of pathways that are not strongly coupled to the receptor are difficult to be detected) cannot be determined.

An interesting observation is that some of the observed pEC₅₀ values are many orders of magnitude larger than the corresponding binding affinities (Fig. 1B). An example is Met-I with a pEC₅₀ of 9.6 for G_{αq} activation (Table 1) versus a pK_i of 5.5 for its binding affinity to the 5-HT_{2A}R (Fig. 1). This difference most likely results from the diverse

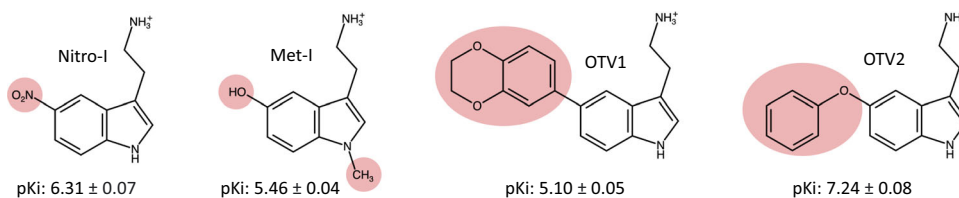


Fig. 1 | Structural derivatives of the endogenous 5-HT_{2A}R agonist serotonin (5-HT). Ligand binding affinities (pK_i) are indicated for Nitro-I, Met-I, OTV1 and OTV2 obtained in [³H]ketanserin competition binding experiments in CHO cells (*n* = 3). The data represent the mean ± SD (see methods section).

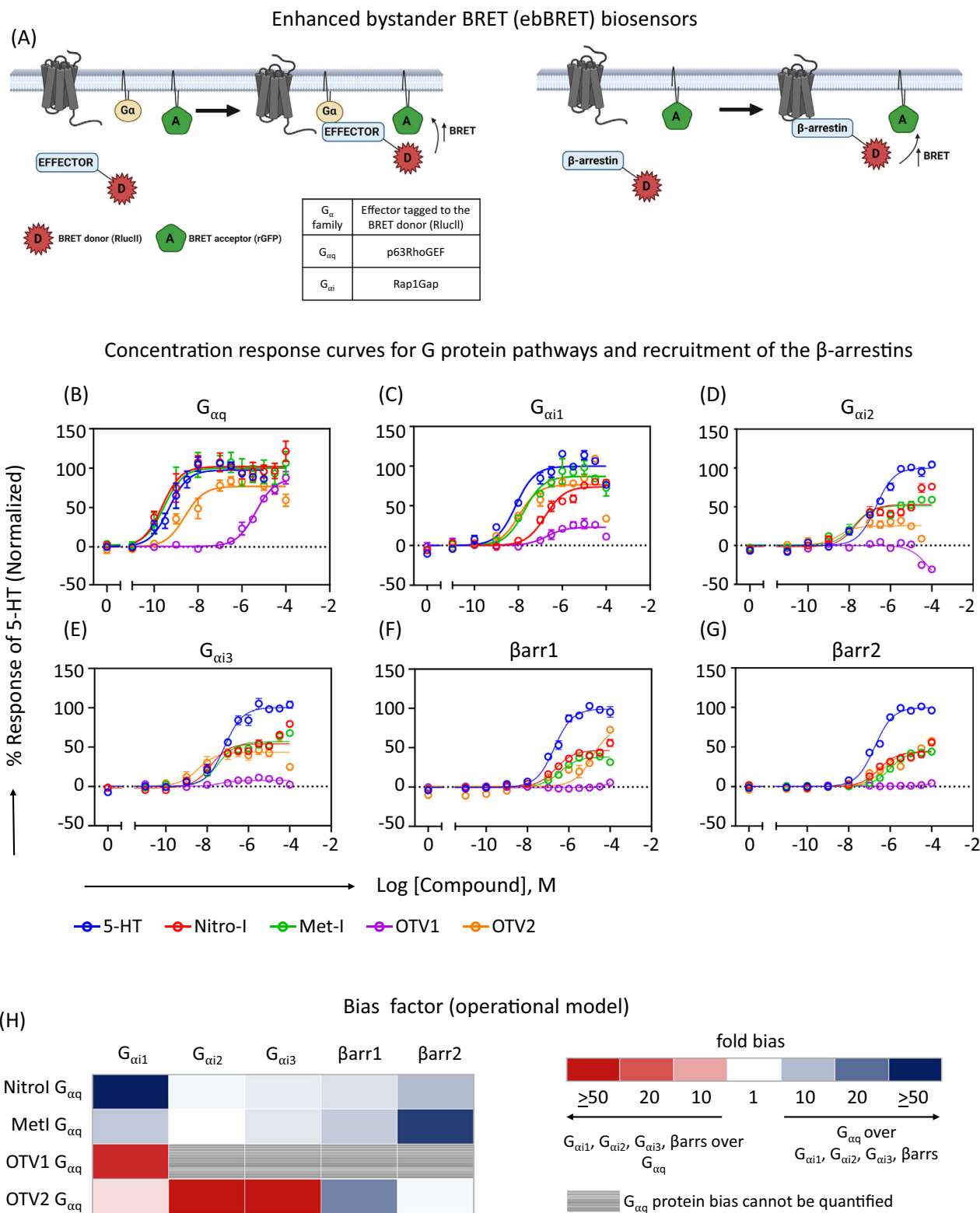


Fig. 2 | G protein coupling and β -arrestin recruitment for Nitro-I, Met-I, OTV1 and OTV2 in living cells. **A** Schematic representation of enhanced bystander BRET (ebBRET) biosensors used to measure G protein activation and β -arrestin (β arr) recruitment in HEK-293 cells, created with BioRender. **B–G** Dose response curves depicting the activity of Nitro-I, Met-I, OTV1 and OTV2 at the different G

protein signaling pathways and for the recruitment of β arr 1 and 2. The ligand-promoted BRET (Δ BRET) was further normalized with respect to the response of 5-HT (mean \pm SEM; $n = 3$). **H** Bias factor for the $G_{\alpha q}$, $G_{\alpha i}$ family and β arr1 and 2. The operational model was used for bias calculations (see method section in supplementary information).

Table 1 | Functional selectivity profile of Nitro-I, Met-I, OTV1, and OTV2 from BRET assays in the agonist mode

	5-HT			Nitro-I			Met-I			OTV1			OTV2		
	pEC ₅₀	E _{max}	log ₁₀ /K _A	pEC ₅₀	E _{max}	log ₁₀ /K _A	pEC ₅₀	E _{max}	log ₁₀ /K _A	pEC ₅₀	E _{max}	log ₁₀ /K _A	pEC ₅₀	E _{max}	log ₁₀ /K _A
G _{αq}	9.75 ± 0.23	101.10 ± 2.37	9.70 ± 0.15	9.65 ± 0.19	102.50 ± 9.81	9.67 ± 0.20	9.55 ± 0.31	98.16 ± 12.19	9.57 ± 0.39	5.38 ± 0.08	86.62 ± 3.72	5.28 ± 0.11	8.35 ± 0.19	75.20 ± 5.12	8.24 ± 0.14
G _{α11}	10.26 ± 0.08	98.03 ± 3.46	9.46 ± 0.06	9.96 ± 0.23	78.67 ± 6.99	9.13 ± 0.13	8.88 ± 0.11	79.73 ± 3.08	8.60 ± 0.12	5.41 ± 0.10	127.30 ± 11.26	5.93 ± 0.15	9.56 ± 0.12	80.31 ± 3.35	8.92 ± 0.12
G _{α14}	9.30 ± 0.10	98.44 ± 5.21	9.14 ± 0.09	8.72 ± 0.15	102.90 ± 5.67	8.73 ± 0.14	8.72 ± 0.11	98.77 ± 4.13	8.72 ± 0.13	5.72 ± 0.13	94.48 ± 5.94	5.64 ± 0.15	9.18 ± 0.25	90.79 ± 6.32	9.13 ± 0.14
G _{α15}	8.10 ± 0.08	99.36 ± 3.22	8.03 ± 0.09	7.61 ± 0.13	107.80 ± 4.62	7.66 ± 1.03	7.22 ± 0.27	98.48 ± 5.40	7.21 ± 0.10	NA	NA	NA	7.55 ± 0.33	60.05 ± 6.63	7.68 ± 0.04
G _{α1}	8.12 ± 0.17	99.92 ± 6.02	8.16 ± 0.15	6.78 ± 0.09	73.92 ± 2.88	6.42 ± 0.15	7.73 ± 0.15	87.12 ± 4.55	7.56 ± 0.15	6.71 ± 0.28	23.21 ± 2.96	5.59 ± 0.44	7.96 ± 0.25	76.81 ± 6.93	7.65 ± 0.18
G _{α2}	6.71 ± 0.08	99.95 ± 3.55	6.70 ± 0.15	7.69 ± 0.22	54.55 ± 4.28	6.73 ± 0.61	7.75 ± 0.16	50.40 ± 2.84	6.90 ± 0.60	NA	NA	NA	8.50 ± 0.38	25.05 ± 3.43	7.23 ± 0.70
G _{α3}	7.16 ± 0.10	100 ± 3.89	7.20 ± 0.10	7.91 ± 0.15	54.48 ± 3.07	7.07 ± 0.18	7.47 ± 0.13	56.76 ± 2.50	6.88 ± 0.17	NA	NA	NA	8.45 ± 0.31	42.55 ± 4.58	7.70 ± 0.23
G _{αA}	7.02 ± 0.08	99.99 ± 3.33	7.01 ± 0.15	7.27 ± 0.24	51.01 ± 4.45	6.64 ± 0.51	7.14 ± 0.19	47.38 ± 3.50	6.25 ± 0.33	NA	NA	NA	8.35 ± 0.25	29.67 ± 2.68	7.76 ± 0.51
G _{αB}	6.98 ± 0.08	99.85 ± 3.46	7.05 ± 0.11	7.25 ± 0.23	45.76 ± 3.87	6.57 ± 0.24	7.12 ± 0.16	47.46 ± 2.89	6.63 ± 0.23	NA	NA	NA	8.04 ± 0.45	40.55 ± 6.64	7.18 ± 0.27
G _{αz}	8.00 ± 0.08	94.48 ± 3.32	8.13 ± 0.08	7.36 ± 0.14	100.30 ± 5.06	8.69 ± 0.13	7.20 ± 0.13	82.95 ± 4.19	8.55 ± 0.10	8.12 ± 1.81	16.44 ± 1.52	4.67 ± 0.90	8.12 ± 0.21	61.83 ± 5.17	7.89 ± 0.31
β-arrestin1	6.71 ± 0.06	99.31 ± 2.59	6.88 ± 0.05	6.65 ± 0.09	46.59 ± 1.95	6.32 ± 0.14	6.44 ± 0.08	38.18 ± 1.40	6.04 ± 0.17	NA	NA	NA	4.80 ± 0.17	76.65 ± 9.22	4.37 ± 0.10
β-arrestin2	6.75 ± 0.04	99.70 ± 1.85	6.84 ± 0.05	6.55 ± 0.11	43.78 ± 2.15	6.15 ± 0.12	6.02 ± 0.05	44.96 ± 1.10	5.63 ± 0.12	NA	NA	NA	6.32 ± 0.15	45.50 ± 3.22	5.44 ± 0.13

NA no activity. Data represent mean ± SEM of 3 independent experiments.

experimental setups including the expression level of receptors or G proteins¹⁵. Interestingly, additional BRET experiments show that receptor expression levels do not affect the observed pEC₅₀ values (Fig. S9). In contrast, we find that increasing levels of G_{αq} significantly increment the apparent potency of Met-I (Fig. S10). This finding demonstrates that the expression level of G protein is a critical parameter that largely contributes to the differences observed between pEC₅₀ of G protein activation and pKi of ligand binding. It further underscores the difficulties associated with comparing data points across distinct experimental setups and could also explain the differences observed between cell-based and ex vivo experiments.

Met-I and OTV1 reduce the basal activity of the G_{αi1} pathway via the 5-HT_{2A}R in postmortem brain tissue

Next, we explored the ability of our molecular probes to modulate the activity of diverse G protein subtypes (G_{αq/11}, G_{αi1}, G_{αi2}, G_{αi3}) in postmortem human brain tissue. For this, we used [³⁵S]GTPγS binding experiments coupled to immunoprecipitation of G_α subunits of heterotrimeric G proteins (Fig. 3A) in postmortem human dorsolateral prefrontal cortex (PFC) membrane-enriched fractions^{16,17}. To confirm that these effects were mediated through 5-HT_{2A}R, the same assays were carried out in the presence of MDL-11,939, a 5-HT_{2A}R-selective neutral antagonist¹⁸ (Fig. 3B–E, Fig. S1, Table 2).

Our study reveals that Nitro-I triggered statistically significant activation of G_{αi1}, G_{αi3} and G_{αq/11}. Among them, only G_{αi1} and G_{αq/11} are 5-HT_{2A}R-mediated, as co-incubation with MDL-11,939 reversed the observed effect completely or partially, respectively (Fig. 3B, Table 2). Met-I modulated the activity of all studied G_α subunit subtypes, with the exception of G_{αi2}. Selective 5-HT_{2A}R inhibition with MDL-11,939 suggests that inverse agonism at G_{αi1} and agonism at G_{αi3}, G_{αq/11} are directly mediated by 5-HT_{2A}R (Fig. 3C, Table 2). In the same way, although OTV1 and OTV2 are able to modulate all studied G_α subunit subtypes (Fig. 3D, E, Table 2), only G_{αi1}, G_{αi3} and G_{αq/11} modulation is 5-HT_{2A}R-mediated, but not G_{αi2} modulation. However, one main difference is related to the observation that Met-I and OTV1 elicit inverse agonism at the G_{αi1} whereas Nitro-I and OTV2 show a G_{αi1} agonism. The overall observed G_{αq/11} activation for tested compounds in postmortem brain samples (Fig. 3B–E) is in line with the activation of the canonical G_{αq} in our BRET experiments in living cells (Fig. 2D). Interestingly, differences are found for the regulation of G_{αi1}, G_{αi2} and G_{αi3} subunit's activity between postmortem brain samples and the cell-based setup. These differences are not surprising considering variations in the experimental environment between postmortem brain samples and cell-based assays. This includes different expression levels of G proteins, 5-HT_{2A}R and other GPCRs. In fact, the presence of other GPCR types has been reported to promote the formation of heteromers which can alter the coupling response of 5-HT_{2A}R. For instance, signaling via the CB₁R-5-HT_{2A}R heteromer promotes G_{αi} coupling and

not the canonical G_{αq} coupling of the 5-HT_{2A}R¹⁹. The presence of other factors in the postmortem tissue *vs* the cell line system could also explain the difference. The fact that Met-I and OTV1 are inverse agonists on G_{αi1} in the human brain but partial agonists for this pathway in the cell-based assays could be related to a higher basal tone for the 5-HT_{2A}R-promoted G_{αi1} activation in the tissue.

To further demonstrate the role of 5-HT_{2A}R in the observed effects in postmortem human brains, tissue homogenates from the brain cortex of wild type (WT) and 5-HT_{2A}R knockout (KO) mice were incubated with Nitro-I, Met-I, OTV1, and OTV2 in [³⁵S]GTPγS binding experiments (Fig. 3F–I, Fig. S2, Table S1). Importantly, these experiments confirm 5-HT_{2A}R-mediated signaling profiles observed in postmortem human PFC. Only small differences are found for the Nitro-I-induced G_{αq/11} activation, which is exclusively mediated through the 5-HT_{2A}R in mice, whereas a partial blockade was observed in human brain with the 5-HT_{2A}R-selective antagonist MDL-11,939.

All in all, our experiments highlight the complex signaling profile elicited by the tested compounds (Fig. 3B–I) that behave as agonists, inverse agonists or show no effect for the different subunit subtypes in homogenates from human PFC or mice brain cortex. Furthermore, we find that the observed coupling profile is often the result of interaction with multiple receptor types, as selective 5-HT_{2A}R antagonism does not always reverse the observed effects. This is also indicated by the finding that some of the effects are still present in 5-HT_{2A}R KO mice brain tissue. Most importantly, we identify two compounds, Met-I and OTV1, that show an inverse agonism effect over the G_{αi1} via the 5-HT_{2A}R. Since different guanosine diphosphate (GDP) concentrations and specific antibodies are used for the detection of each G_α subunit, results obtained from this methodological approach are semiquantitative. Thus, no quantitative comparisons can be made between the different studied subunits, no bias factor can be calculated, and only the effects of different compounds over the same subunit can be compared.

G_{αi} agonism is implicated in psychosis-related effects

To interrogate the implication of specific 5-HT_{2A}R-mediated pathways in psychosis-related behavior, we investigated the effects of in vivo administration of our test compounds in mice on the head twitch response (HTR). The HTR serves as a behavioral proxy in rodents for human psychedelic effects, and can be used to discriminate hallucinogenic and non-hallucinogenic 5-HT_{2A}R agonists^{9,20–25}. Thus, increasing doses of Nitro-I, Met-I, OTV1 or OTV2 were administered intracerebroventricularly (ICV), as well as DOI, a classic psychedelic 5-HT_{2A}R agonist, chosen as control. In a first step, we confirmed that our test compounds are not lethal or produced any physiological or neurotoxicity symptoms in mice for tested doses by the Irwin test (see Methods).

As expected, the HTR is significantly increased by our reference compound DOI with respect to vehicle-treated animals (Fig. S3, inset). We found that Nitro-I and OTV2, compounds triggering a

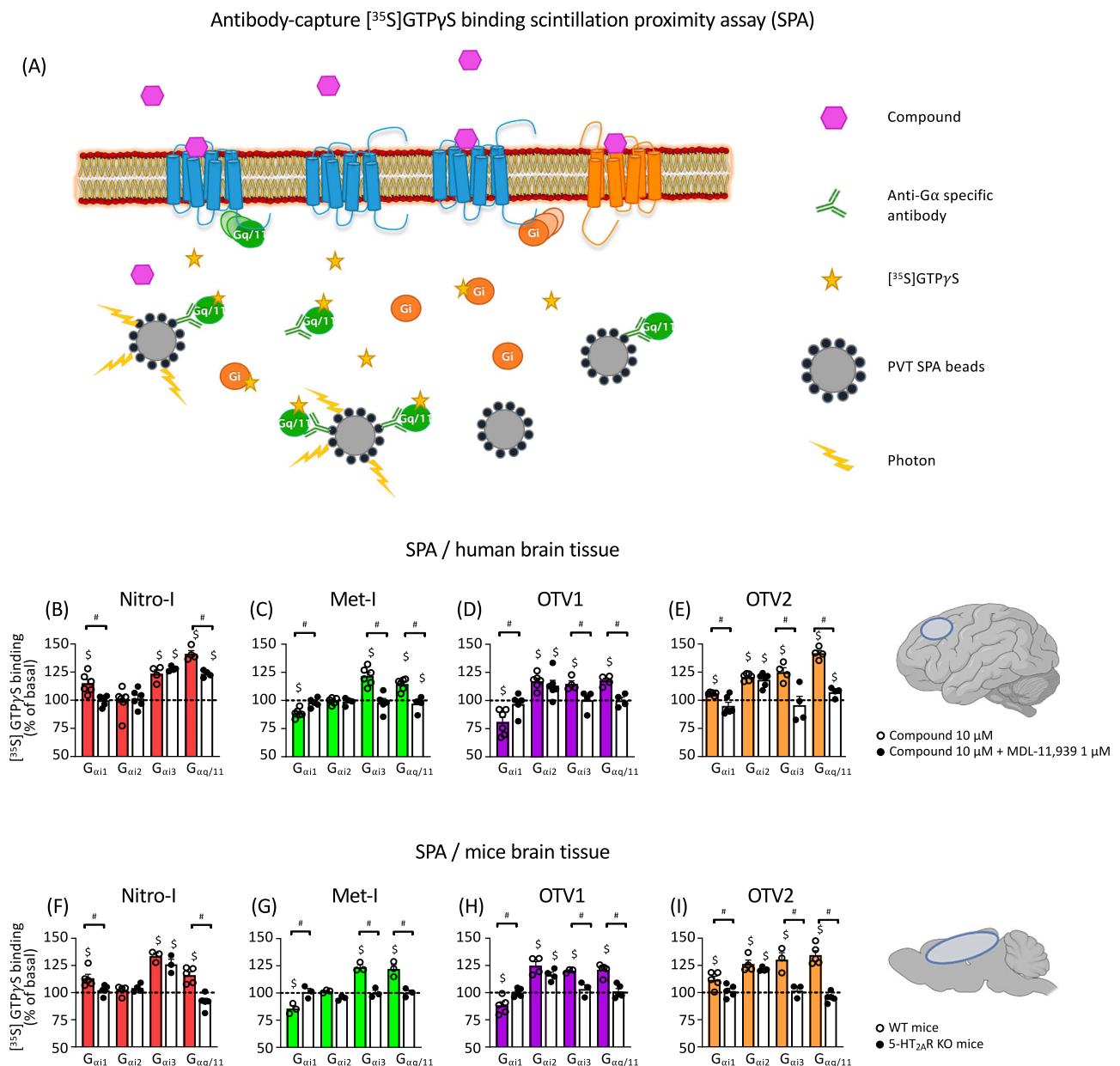


Fig. 3 | Antibody-capture ^{35}S GTP γ S binding scintillation proximity assay (SPA). **A** Schematic representation of the SPA methodology, created using BioRender. SPA allows the determination of the activation level of different G α subunit subtypes present in postmortem brain tissue thanks to the selective immunoprecipitation of each of them and their coupling to protein A-coated polyvinyltoluene SPA beads. Modulation of specific ^{35}S GTP γ S binding to G α_{i1} , G α_{i2} , G α_{i3} and G $\alpha_{q/11}$ proteins by 10 μM Nitro-I (**B**), Met-I (**C**), Otava 3575001 (OTV1) (**D**) and Otava 3736689 (OTV2) (**E**) in human prefrontal cortex both in the absence (colored bars) and in the presence (white bars) of the 5-HT_{2A}R antagonist MDL-11,939. Basal values of specific ^{35}S GTP γ S binding to the different G proteins are expressed as 100% and stimulatory/inhibitory effects on the respective basal are shown. Individual dots represent different assays 4–6 carried out for each subunit/condition performed in

duplicate or triplicate. White dots represent data for the drug-alone condition, and black dots represent data for the drug + MDL condition (**B–E**). $^{\#}p < 0.05$ vs 100%; $^{\$}p < 0.05$ vs incubation in the presence of 1 μM MDL-11,939 (*t*-test). Modulation of specific ^{35}S GTP γ S binding to G α_{i1} , G α_{i2} , G α_{i3} and G $\alpha_{q/11}$ proteins by 10 μM Nitro-I (**F**), Met-I (**G**), OTV1 (**H**) and OTV2 (**I**) in brain cortex tissue from WT (colored bars) and 5-HT_{2A}R KO mice (white bars). $^{\#}p < 0.05$ vs 100%; $^{\$}p < 0.05$ WT vs 5-HT_{2A}R KO (*t*-test). Basal values of specific ^{35}S GTP γ S binding to the different G proteins are expressed as 100%, and stimulatory/inhibitory effects on the respective basal are shown. Individual dots represent the different assays (3–5) for each subunit performed in duplicate or triplicate. White dots represent data for WT mice and black dots represent data for KO mice (**F–I**).

5-HT_{2A}R-mediated G α_{i1} , G α_{i3} and G $\alpha_{q/11}$ agonism in postmortem brain assays, significantly increased HTR as compared to vehicle administration (Fig. S3A, D). Importantly, this effect is absent in 5-HT_{2A}R KO mice (Fig. 4A, D), indicating a 5-HT_{2A}R-dependent mechanism, and supporting other data showing that the 5-HT_{2A}R is necessary for the expression of HTR²¹.

Interestingly, Met-I and OTV1, which showed 5-HT_{2A}R-mediated G α_{i1} inverse agonism in brain tissue experiments, do not increase HTR at any

of the doses tested (Fig. S3B, C) in WT or 5-HT_{2A}R KO mice (Fig. 4B, C). Note that in addition to inverse agonism of G α_{i1} , both compounds also stimulate the activity of G α_{i3} and G α_{q} subtypes. To evaluate the possible involvement of G α_{i1} , G α_{i3} and G α_{q} in the regulation of psychosis-related effects (i.e. HTR) through 5-HT_{2A}R stimulation, we used two different methodological approaches. On one hand, we carried out pharmacological inhibition of G $\alpha_{q/11}$ by ICV administration of YM-254890. On the other hand, we reduced the expression level of G α_{i1} and G α_{i3} genes,

Table 2 | Normalized [³⁵S]GTPγS binding values for G_{αi1}, G_{αi2}, G_{αi3}, and G_{αq/11} in postmortem human prefrontal cortex membrane homogenates

	Nitro-I					Nitro-I + MDL					Met-I					Met-I + MDL						
	Mean	±	SEM	n	p value	Mean	±	SEM	n	p value	p value	Mean	±	SEM	n	p value	Mean	±	SEM	n	p value	p value
G _{αi1}	114.9	±	3.5	6	0.008	100.0	±	1.8	6	ns	0.006	88.7	±	1.6	6	0.001	98.2	±	1.8	5	ns	0.004
G _{αi2}	99.2	±	4.8	6	ns	101.5	±	3.2	6	ns	ns	99.5	±	1.4	5	ns	99.0	±	1.6	4	ns	ns
G _{αi3}	123.4	±	3.4	4	0.006	127.9	±	1.0	4	<0.001	ns	121.6	±	3.2	6	0.001	98.0	±	3.8	5	ns	0.001
G _{αq/11}	141.3	±	2.9	4	0.001	123.5	±	1.5	4	0.001	0.004	114.4	±	2.1	6	0.001	97.2	±	2.7	5	ns	0.001
	OTV1					OTV1 + MDL					OTV2					OTV2 + MDL						
	Mean	±	SEM	n	p value	Mean	±	SEM	n	p value	p value	Mean	±	SEM	n	p value	Mean	±	SEM	n	p value	p value
G _{αi1}	80.6	±	4.6	6	0.008	97.0	±	4.2	5	ns	0.027	105.9	±	0.5	6	<0.0001	95.0	±	3.2	6	ns	0.018
G _{αi2}	117.2	±	2.7	6	0.001	113.3	±	4.7	6	0.036	ns	120.8	±	1.2	6	<0.0001	118.2	±	2.3	6	0.001	ns
G _{αi3}	114.7	±	2.8	4	0.013	100.3	±	4.6	4	ns	0.044	124.9	±	4.1	4	0.009	95.7	±	7.8	4	ns	0.024
G _{αq/11}	117.6	±	2.3	4	0.005	100.0	±	2.8	4	ns	0.003	141.7	±	2.6	4	0.001	107.2	±	2.2	4	0.045	<0.0001

An agonist behavior results in a significant increase over basal binding, while an inverse agonist reduces it and an antagonist would not modify it. Results were analyzed by two-tailed Student's t-test (one-sample) vs basal values (expressed as 100%) or by two-tailed Student's t-test (two-sample) between conditions (presence vs absence of MDL-11,939; italicized p values). p values under 0.05 are highlighted in bold. Data are described as mean ± SEM values. ns: non-significant.

GNAI1 and GNAI3 respectively, by the ICV administration of specific antisense oligonucleotides (ODNs). OTV2 was selected as a model drug for these experiments, as it induces HTR and shows a 5-HT_{2A}R-mediated activation of G_{αi1}, G_{αi3} and G_{αq} in postmortem brain tissue.

Importantly, we find that OTV2-induced HTR at the dose of 0.05 μg/μl was not modulated by G_{αq/11} inhibition using YM-254890 (Fig. 4E). Instead, decreasing protein levels for both G_{αi1} and G_{αi3} using ODNs abrogated the OTV2-induced HTR (Fig. 4F). We confirmed that G_{αi1} and G_{αi3} protein levels were significantly decreased in mice after chronic treatment with G_{αi1}- or G_{αi3}-ODNs compared to ODN-RDN (i.e., a random oligo) using Western blot analysis (Fig. S4), whereas no change was observed for the expression levels of G_{αq/11}. The specificity of the used antibodies has been previously demonstrated¹⁶. Surprisingly, although the used ODNs had been previously described in the literature²⁶, a cross-effect of G_{αi1} ODN and G_{αi3} ODN treatment over both G_{αi1} and G_{αi3} protein expression levels was observed in our hands (Figure S4). Therefore, we are not able to discriminate between G_{αi1}- and G_{αi3}- mediated effects with the currently existing reagents.

Altogether, our results provide evidence that the activation of G_{αi} protein family-coupled signaling pathways (G_{αi1} and/or G_{αi3}) via the 5-HT_{2A}R is a main contributor to psychosis-related effects in mice. Although our data suggest that G_{αi1}-activation is necessary for this effect, we cannot completely exclude mechanisms other than G_{αi/o} activation in mediating HTR. Previous studies describe the involvement of other coupling partners including G_{αq}^{25,27–30}, although there are also studies showing that G_{αq} KO mice inhibit only partially HTR²⁷, suggesting additional contributing mechanisms in HTR. Moreover, studies have reported the involvement of G_{αs} proteins³⁰, G_{βγ} subunits³¹, and β-arrestins^{11,12} in HTR.

Long-term memory performance is linked to 5-HT_{2A}R-induced G_{αq} activation

To investigate the ability of our compounds to modulate cognitive performance via the 5-HT_{2A}R, we carried out the novel object recognition (NOR) test in WT and 5-HT_{2A}R KO mice. Indeed, we find that Met-I and OTV1 induce significant long-term memory deficits in WT mice at both doses tested through a 5-HT_{2A}R-dependent mechanism (Fig. 4H, I). Interestingly, OTV2 produces long-term memory deficits in WT mice only at the lower dose, and this effect is absent in KO mice (Fig. 4J). To our surprise, we find that Nitro-I is the only compound that does not induce long-term memory deficits (Fig. 4G).

To interrogate which pathway is associated with these effects over cognition, we chose again OTV2, our model compound able to induce long-term cognitive impairment in addition to HTR. For discriminating which of the G_α protein subtypes (G_{αi1}, G_{αi3} and G_{αq}) activated by OTV2

through a 5-HT_{2A}R-mediated mechanism in human and mouse brain tissue are implicated in these memory effects, we used again the two approaches previously described in the HTR section: (i) reduction of protein expression levels of G_{αi1} and G_{αi3} via ODN administration and (ii) G_{αq} pharmacological inhibition using YM-254890.

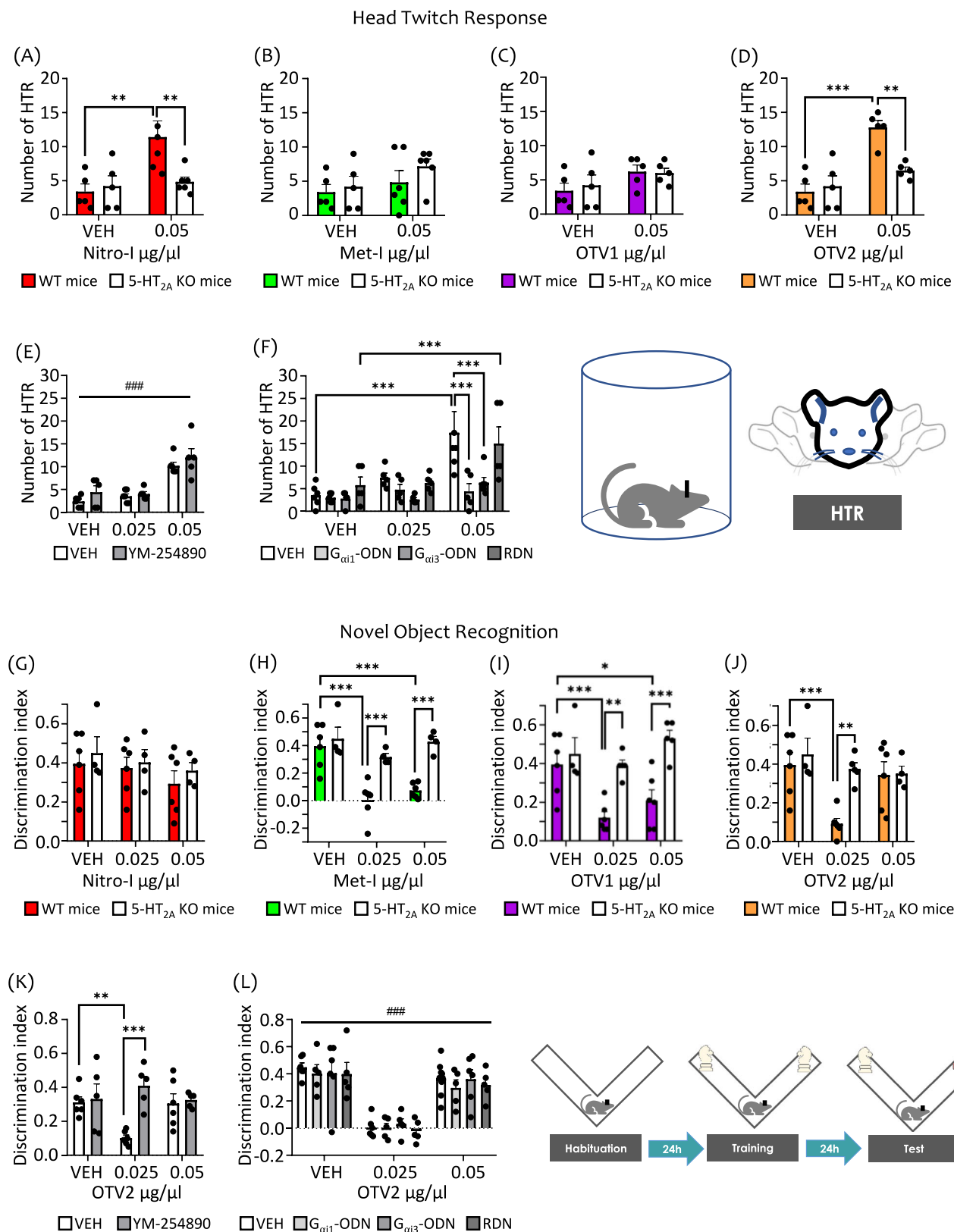
We find that reducing the protein levels of G_{αi1} and G_{αi3} via ODNs did not influence long-term memory deficits induced by OTV2 at the dose of 0.025 μg/μl (Fig. 4L). Instead, inhibiting G_{αq} activation with YM-254890 abrogated OTV2-induced long-term memory deficits (Fig. 4K). These results provide first evidence that long-term memory performance is linked to modulation of the G_{αq}-coupled pathway via the 5-HT_{2A}R. Importantly, our data suggest further that cognitive deficits require other co-factors/events in addition to G_{αq} activation. This can be concluded from the observation that although Nitro-I also activates G_{αq} in cell-based and brain tissue experiments, it does not elicit cognitive deficits.

In a final experiment, we also evaluated whether our compounds induced anhedonia, one of the features of depression, and our results showed that none of the doses administered acutely evoked this behavior in WT or KO mice (Fig. S5).

Ligands with differential 5-HT_{2A}R coupling profiles and in vivo responses establish distinct ELC2 interactions

In the previous experiments, we have employed signaling probes that are structurally closely related to the endogenous neurotransmitter 5-HT. One main difference between these signaling probes are diverse substituents in position 5 of the indole scaffold, which proved to alter the 5-HT_{2A}R coupling profile in living cells (Fig. 2), and in postmortem brain tissue (Fig. 3) and behavioral responses (Fig. 4).

Molecular dynamics (MD) simulations have been shown to be a valuable tool for interrogating structural and dynamic events linked to GPCR function^{32–34} including signaling bias³⁵. Here, we exploited this approach to elucidate the structural determinants that may be responsible for the different in vitro and in vivo responses of the 5-HT_{2A}R. For this, we constructed 3D structural models of the complexes by docking all ligands into the orthosteric binding site of the 5-HT_{2A}R and subjected each complex to MD simulation. Structural inspection of the most representative clusters found in simulations reveals that the positioning of the main tryptamine scaffold of all compounds resembles the experimentally solved tryptamine pose of serotonin in the 5-HT_{1A}R (PDB id 7E2Y) with the following interactions of high contact frequencies (Fig. 5A, B): (i) a salt bridge with D3.32 and (ii) a hydrophobic sandwich formed of V3.33, F6.51 and F6.52. In fact, these positions have been corroborated by numerous mutational studies for tryptamine, 5-hydroxytryptamine and other closely related derivatives



(i.e., V3.33³⁶, F6.51, and F6.52^{37–39}). With this central scaffold in place, extension in position 5, as observed in OTV1 (1,4 benzodioxin) and OTV2 (phenoxy), are oriented towards the extracellular loop 2 (ECL2) where they result in increased contact frequencies (Fig. 5C). This interaction is mediated by hydrophobic interactions, in particular with L228 and L229, but also by additional hydrogen bonds with the

backbone of L229 in the case of OTV1. The role of ECL2, specifically L229, mediating interactions with bulkier compounds in serotonin receptors has been reported by Wacker et al.⁴⁰.

Interestingly, we observe that differential ligand-receptor interactions are associated with distinct ligand binding affinities at the 5-HT_{2A}R in cell-based assays (Fig. 5D). The highest affinity for 5-HT_{2A}R

Fig. 4 | Head twitch response (HTR) and long-term novel object recognition (NOR). HTR in wild-type (WT) and 5-HT_{2A}R knockout (KO) mice following ICV administration of (A) Nitro-I, (B) Met-I, (C) OTV1, and (D) OTV2, or vehicle (VEH). The increase in HTR induced by Nitro-I and OTV2 at the dose of 0.05 µg/µl was absent in KO mice. **E** ICV administration of YM-254890 (16 µM) did not modulate the increase in HTR induced by OTV2 at the dose of 0.05 µg/µl. **F** ICV administration of specific antisense oligonucleotides (ODN), G_{αi1}-ODN, G_{αi3}-ODN, but not control random oligonucleotides (RDN) blocked HTR induced by OTV2 at the dose of 0.05 µg/µl. NOR memory test in WT and 5-HT_{2A}R KO mice following ICV administration of (G) Nitro-I, (H) Met-I, (I) OTV1, and (J) OTV2 or vehicle (VEH). In WT mice,

Met-I and OTV1 induced memory deficits at the dose of 0.025 and 0.05 µg/µl, and OTV2 was effective only at the dose of 0.025 µg/µl. These effects were abrogated in KO mice. Nitro-I did not trigger memory deficits at any of the doses tested. **K** YM-254890 (16 µM) abrogated the memory deficits induced by OTV2 at the dose of 0.025 µg/µl. **L** ICV administration of G_{αi1}-ODN, G_{αi3}-ODN, or the control RDN sequence did not modulate the memory deficits induced by OTV2 at the dose of 0.025 µg/µl. The data represent mean ± SEM. The number of mice used in the experiments (n) corresponds to the individual points in the graph. **p < 0.01, ***p < 0.001, and ****p < 0.0001 (main effect of treatment). Two-way ANOVAs followed by Fisher's post-hoc test.

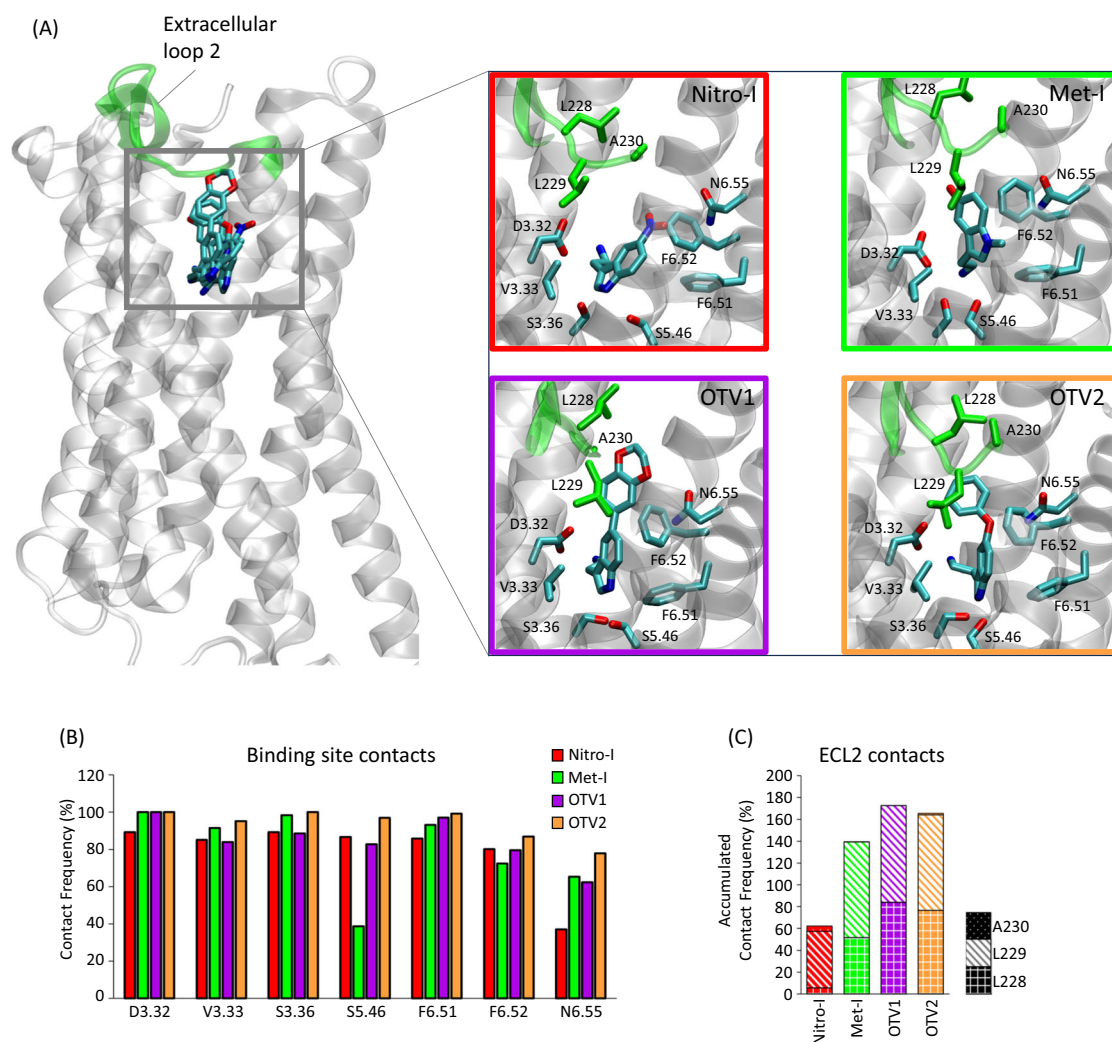


Fig. 5 | In silico modeling of the ligand-5-HT_{2A}R interactions for Nitro-I, Met-I, OTV1, and OTV2. **A** 3D model of the ligand-5-HT_{2A}R interactions for Nitro-I, Met-I, OTV1, and OTV2. The ECL2 and included residues are highlighted in green. **B** The contact frequency (%) of residues in the transmembrane region of the receptor for each ligand. Contact frequencies have been computed for the

main conformational cluster (see Methods) extracted from three replicates of 500 ns MD simulations (3 × 500 ns). **C** Accumulated contact frequency of residues in the ECL2 for each ligand computed for the main cluster extracted from three replicates of 500 ns MD simulations (3 × 500 ns).

is found for OTV2 which exposes a phenoxy substituent in position 5 of the indole fragment. Elongation of this position to a benzodioxan dramatically reduces ligand binding affinity as seen for OTV1. In addition, we observe that introducing a methyl substituent at the heteroaromatic nitrogen in position 1 is not favorable for ligand binding affinity, as observed for Met-I. One could speculate that ligand binding affinities are correlated with the total amount of receptor contacts (i.e. pocket plus ECL2 contacts). However, this is not the case as specific contact types (e.g. hydrogen bonds or Van der Waals)

contribute differently to the binding affinity which is not taken into account when computing the total number of contacts.

Nevertheless, the type of substitution in position 5 of the indole scaffold and corresponding ECL2 contacts seem to alter 5-HT_{2A}R coupling in living cells (Fig. 2). Compounds with small-sized substitutions in position 5 (i.e., Nitro-I and Met-I) show overall G_{αq} physiology-bias (compared to 5-HT) over the tested G_{αi} proteins as well as β-arrestin 1 and 2 (Fig. 2H). Changes are observed upon extension of position 5. Both, OTV1 (5-benzodioxin substituent) and OTV2

(5-phenoxy substituent) show a $G_{\alpha_{i1}}$ bias over the canonical $G_{\alpha_{q}}$ protein (Fig. 2H). Our structural models of ligand binding suggest that this change in coupling profile could be related to increased interaction with the ECL2 via the extended substituent in position 5 (Fig. 5C).

Structural modifications of the indole scaffold also significantly impact the 5-HT_{2A}R-induced G protein activation profile in human brain tissue: Nitro-I ($G_{\alpha_{i1}}$, $G_{\alpha_{q/11}}$ agonism), Met-I (inverse $G_{\alpha_{i1}}$ agonism and $G_{\alpha_{i3}}$, $G_{\alpha_{q/11}}$ agonism), OTV1 ($G_{\alpha_{i1}}$, $G_{\alpha_{i3}}$, $G_{\alpha_{q/11}}$ agonism) and OTV2 (inverse $G_{\alpha_{i1}}$ agonism and $G_{\alpha_{i3}}$, $G_{\alpha_{q/11}}$ agonism). For instance, our data suggest that increased ECL2 contacts (Met-I, OTV1, OTV2, Fig. 5C) promote $G_{\alpha_{i3}}$ activation in brain tissue (Fig. 3C–E) compared to Nitro-I (Fig. 3B). One of the most important structural observations is that the regulation of the psychosis-associated $G_{\alpha_{i1}}$ pathway can be mediated by diverse mechanisms. On one hand, we find that differential interaction within the ECL2 (Fig. 5A, C) can convert a $G_{\alpha_{i1}}$ agonism of OTV2 (hydrophobic ECL2 interaction via 5-phenoxy) (Fig. 3E) into a $G_{\alpha_{i1}}$ inverse agonism as observed for OTV1 (polar ECL2 interaction via 5-benzodioxan) (Fig. 3D). In addition, we find that $G_{\alpha_{i1}}$ agonism can also be induced by compounds with a relatively low number of ECL2 contacts (Nitro-I, Figs. 3B, 5C).

Based on this finding and our structural models, we propose that $G_{\alpha_{i1}}$ agonism does not require strong ECL2 contacts, whereas $G_{\alpha_{i1}}$ inverse agonism can be induced via differential interactions with the ECL2. In fact, this is in line with structural observations for the hallucinogenic compound LSD (PDB 6WGT) that stimulates $G_{\alpha_{i/o}}$ coupling⁹ compared to the non-hallucinogenic compound lisuride (PDB 7WC7) with no $G_{\alpha_{i/o}}$ coupling through 5-HT_{2A}R⁹. Both compounds are structurally closely related with a highly similar binding mode but show differences in their interaction frequencies with the ECL2 in MD simulations (Fig. S6). Finally, another relevant structural observation is that compounds that induce cognitive deficits (Met-I, OTV1 and OTV2) are characterized by pronounced contacts with the ECL2 when compared to Nitro-I.

Overall, our structural insights can have important implications for the rational design of drug candidates with a tailored signaling profile and in vivo response applied to the treatment of psychiatric diseases.

Discussion

In this study, we have investigated the complex coupling profile of the 5-HT_{2A}R in living cells and in postmortem brain tissue. Furthermore, in mouse models we tested the ability of several 5-HT_{2A}R agonists to modulate behaviors that have been associated with SCZ, including psychosis-related effects, anhedonia and cognitive deficits. For this, we used small molecular probes closely related to the endogenous agonist 5-HT and monitored their impact on receptor coupling preferences. The potential of such a strategy has been previously demonstrated by us for exploring the coupling bias of the dopamine D₂ receptor³⁵. Exploiting this framework, we were able to detect structural determinants at the level of receptor binding that could relate to specific 5-HT_{2A}R-induced responses. Specifically, we find that the degree of ligand interaction with the ECL2 has a dramatic impact on the receptor's potency and efficacy to couple to different G protein subtypes in living cells (Fig. 2). This in turn translates into specific physiology-bias profiles for different coupling pathways. For instance, small 5-HT-like compounds (Nitro-I, Met-I) show an overall $G_{\alpha_{q}}$ bias over the $G_{\alpha_{i}}$ family and β -arrestins 1 and 2 (Fig. 2H), whereas extensions in position 5 (OTV2) can convert the coupling preference to the $G_{\alpha_{i}}$ family over the $G_{\alpha_{q}}$ in living cells (Fig. 2H). A specific property of this molecular extension is to promote increased interactions with ECL2 (Fig. 5C) which is potentially responsible for an altered signaling response. In fact, this is in line with a study from Wacker et al.⁴⁰, showing that mutational modifications in the ECL2 of the 5-HT_{2B}R drive ligand binding kinetics and receptor response in cell-based assays⁴⁰. Of note, our study goes beyond cell-based responses and also interrogates the ligand-mediated impact on

signaling in native brain tissue. Our data suggest that one possible mechanism for modulating agonism (OTV2, Fig. 3E) or inverse agonism (OTV1, Fig. 3D) of the $G_{\alpha_{i1}}$ pathway involves differential interactions with the ECL2 (Fig. 5C). Interestingly, this finding goes along with structural observations for the hallucinogenic LSD ($G_{\alpha_{i/o}}$ stimulation) and the non-hallucinogenic lisuride (no $G_{\alpha_{i/o}}$ stimulation)^{9,41–43}. Experimentally solved structures of these two closely related compounds bound to the 5-HT_{2A}R show main differences in ECL2 interactions that could be responsible for the differential $G_{\alpha_{i/o}}$ family coupling properties (Fig. S6). In contrast to this, ECL2 contacts seem to be of less relevance for $G_{\alpha_{i1}}$ agonism, as demonstrated by Nitro-I, which shows a marked reduction of ECL2 contacts. The obtained structural insights are of high importance for the tailored design of compounds with a specific coupling profile. Of note, our structural observations are limited to compounds with a 5-HT scaffold. Taking into account the complexity of signaling responses, we cannot exclude the existence of additional mechanisms that can drive the observed effects.

Ultimately, to examine the impact of different 5-HT_{2A}R signaling profiles on behavioral responses, we moved to in vivo experiments evaluating psychosis-related effects, cognitive deficits, and depression-like behavior induced by our probes^{12,20–24,44}.

Interestingly, the present results demonstrate that compounds that elicit HTR (Nitro-I and OTV2, Fig. 4A, D) are able to induce activation of the $G_{\alpha_{i1}}$ subunit (Fig. 3B, E), while compounds that did not produce HTR (Met-I and OTV1, Fig. 4B, C) show inverse agonism towards $G_{\alpha_{i1}}$ in both human (Fig. 3C, D) and mouse brains (Fig. 3G, H). Importantly, the implication of $G_{\alpha_{i1}}$ in HTR (and thus psychosis-related effects) is further corroborated by our finding that a reduction of the expression levels of $G_{\alpha_{i1}}$ together with $G_{\alpha_{i3}}$ reversed 5-HT_{2A}R-mediated HTR (Fig. 4F). Although no discrimination between the roles of $G_{\alpha_{i1}}$ and $G_{\alpha_{i3}}$ could be made in this experiment, our data suggest that $G_{\alpha_{i1}}$ activation is driving psychosis-related effects as found in Nitro-I and OTV2 based on: (i) only compounds that promote HTR (Nitro-I and OTV2) activate $G_{\alpha_{i1}}$ while others do not (Met-I and OTV1) and (ii) all studied compounds (Nitro-I, Met-I, OTV1, OTV2) activate $G_{\alpha_{i3}}$ independently of their ability to induce/not induce pro-psychotic effects suggesting a marginal implication of $G_{\alpha_{i3}}$ in pro-psychotic effects. Future studies with selective inhibitory tools are required to further investigate the specific implication of $G_{\alpha_{i1}}$ in the psychosis-related effects. It is worth noting that our observation is in agreement with previous findings suggesting that both pro-hallucinogenic and anti-hallucinogenic properties of 5-HT_{2A}R drugs depend on the modulation of $G_{\alpha_{i/o}}$ proteins and their downstream pathways. However, these studies do not further differentiate the precise G protein subunits involved in these processes^{9,45}.

Altogether, our findings indicate that inhibition of 5-HT_{2A}R-mediated $G_{\alpha_{i1}}$ activity could be a promising strategy to selectively reduce pro-psychotic symptoms. Moreover, this approach could down-regulate the supersensitivity of the 5-HT_{2A}R coupling to $G_{\alpha_{i1}}$ -proteins (but not to $G_{\alpha_{q/11}}$), which has been reported to occur in postmortem brains of subjects with schizophrenia⁴¹. On the other hand, Met-I, Nitro-I and OTV2 exhibit similar efficacy/potency for recruiting β -arrestin 1 and 2 in BRET assays, but only Met-I and OTV2 elicited HTR in mice. These findings suggest that activation of β -arrestin may be necessary, but not sufficient for the appearance of HTR (see supplemental section 2).

The 5-HT_{2A}R is also a key player in 5-HT's regulation of learning and memory^{44,46}. Previous studies have investigated the effect of structurally diverse 5-HT_{2A}R ligands in these processes (see supplemental section 3). However, to our knowledge, no study has investigated the implication of specific 5-HT_{2A}R-induced pathways in cognition. Interestingly, examining our 5-HT_{2A}R signaling probes, we find that Met-I, OTV1 and OTV2 but not Nitro-I induced 5-HT_{2A}R mediated long-term memory deficits in WT mice (Fig. 4G–J), mirroring the alterations in cognitive processing in SCZ. Most importantly, our experiments provide evidence that $G_{\alpha_{q}}$ is a critical element in mediating cognitive

processes via the 5-HT_{2A}R, as its pharmacological inhibition reversed the observed long-term memory alterations in mice (Fig. 4K).

Ultimately, our study highlights the challenges in multi-disciplinary research related to the fact that data are often not completely comparable between different experimental setups. Recognizing this divergence in data becomes paramount, as it not only informs researchers about the existing challenge but also serves as a means to elucidate the extent of *in vitro*, *in vivo* and human data alignment. In addition, the differences observed between these setups can have significant implications for gaining a better understanding of the disease mechanisms underlying schizophrenia (e.g. diverse expression levels of coupling partners, etc.).

In conclusion, widely used atypical antipsychotics usually target hallucinations and paranoid thinking, but their beneficial effects on cognitive symptoms are controversial⁴⁷. In addition, current treatments can induce severe side effects which are potentially the result of indiscriminate inhibition/activation of several pathways that can be initiated by one receptor target. Our findings highlight that 5-HT_{2A}R pathway-biased antagonists/inverse agonists that selectively target G_{o1} pathways, and specifically the G_{o1i}, could improve positive symptoms without affecting cognitive processing. In contrast, drugs that selectively block G_{oq/11} signaling could be good therapeutic agents for patients that suffer from cognitive disturbances. Importantly, our work provides structural insights into ligand-receptor interactions, which are of high relevance for the rational design of drugs with desired therapeutic profiles. Beyond this, our work highlights the complexity of GPCR signaling and the relevance of G protein-specific mechanisms for the therapeutic response, which has to be considered for future drug development efforts of more efficient and safer drugs in the treatment of psychiatric diseases.

Methods

Ethical statement

Animal procedures were carried out following the standard ethical guidelines (European Communities Directive 86/609 EEC) and approved by the local ethical committee (CEEA-PRBB).

Human brain samples were obtained at autopsy in the Basque Institute of Legal Medicine, Bilbao, Spain, in compliance with Spanish policies of research and ethical boards for postmortem brain studies. According to applicable laws, samples were obtained by opting-out policy and absence of compensation for tissue donation. The Project was approved by the Institutional Review Board (IRB) of the University of the Basque Country UPV/EHU (CEISH-UPV/EHU, Ref. M10-2019-230).

Virtual screen for 5-HT_{2A}R ligands

Four virtual screens were conducted with the ZINC database⁴⁸ of commercially available 'lead-like' compounds at the orthosteric binding site of 5-HT_{2A}R using four different conformational ensembles derived from the previous publication³. The Glide module in Schrödinger was employed to implement the hierarchy screening workflow⁴⁹. After completing the first step in the quick HTVS mode, the top 100,000 solutions were chosen for the next screen using the Standard Precision (SP) procedure, which uses a more precise scoring function and slower but thorough ligand conformational sampling. To guarantee that the important ligand-protein interactions were captured, the H-bond constraints to D3.32, N6.55, and S5.46 were applied. The most promising compounds were then chosen after visually evaluating the remaining top-ranked compounds based on the interactions between ligands and proteins, shape complementarity, lead-like characteristics, lack of potentially reactive and PAINS groups, and chemical diversity. The experimental validation led to the identification of the molecules OTV1 and OTV2 - two structurally related compounds of Met-I and Nitro-I, which emerged from our previous study³.

Drugs, antibodies, and reagents

The following ligands were used: 2-[5-(2,3-dihydro-1,4-benzodioxin-6-yl)-1H-indol-3-yl]ethan-1-amine Hydrochloride (Otava 3575001; OTV1) and 2-(5-phenoxy-1H-indol-3-yl)ethan-1-amine hydrochloride (Otava 3736689; OTV2) from Otava Chemicals. 2-(5-nitro-1H-indol-3-yl)ethan-1-amine hydrochloride (Nitro-I), 3-(2-aminoethyl)-1-methyl-1H-indol-5-ol hydrochloride (Met-I) and (±)-2,5-dimethoxy-4-iodoamphetamine hydrochloride (DOI HCl) from Sigma-Aldrich Merck. α-phenyl-1-(2-phenylethyl)-4-piperidinemethanol (MDL-11,939) from Bioscience (UK). MDL-11,939 was chosen as a selective 5-HT_{2A}R *vs* 5-HT_{2CR} antagonist^{50,51}. [³⁵S]GTPγS was purchased from Perkin Elmer Life Sciences (Boston, USA). Other reagents for SPA were obtained from Sigma-Aldrich and Perkin Elmer Life Sciences. The antibodies used for *in vitro* functional assays are further described in Supplementary Section 4 and in Table S2.

In behavioral experiments, Nitro-I, Met-I, OTV1, and OTV2 (0.025, 0.05, 0.1, and 0.5, μg/μl) were diluted in 99% saline with 1% DMSO (Sigma-Aldrich Merck), (±)DOI (0.1 μg/μl) was diluted in saline. These compounds were administered intracerebroventricularly (ICV) at a volume of 5 μl. The G_{oq/11} inhibitor YM-254890 (YM, FUJIFILM Wako Pure Chemical Co) was reconstituted with DMSO to provide a stock solution of 1 mM. The stock solution was diluted with saline to a final concentration of 16 μM and administered ICV at a volume of 2.5 μl. The antisense oligodeoxynucleotides (ODNs) that inhibit G_{o1i} and G_{o13} and a random oligo (ODN-RD) that served as a control (Sigma-Aldrich Merck) were reconstituted with Milli-Q water to provide a stock solution in the appropriate concentrations for the ICV administration of the different doses at a volume of 2.5 μl. Sequences were as follows: ODN-G_{o1i}: 5'-G*C*TGTCCTCCACAGTCTCTTTATGACGCCG*G*C-3', corresponding to nucleotides 588–621 of the GNAI1 gene sequence. ODN-G_{o13}: 5'-G*C*CATCTCGCCATAAACGTTAATCACGCCT*G*C-3', corresponding to nucleotides 554–587 of the GNAI3 gene sequence. These sequences showed no homology to other relevant cloned proteins (GeneBank database). ODN-RD with the sequence 5'-C*C*CTTATTACTACTTTC*G*C-3'²⁶.

Bioluminescence resonance energy transfer assay (BRET)

To measure activation of the different G protein pathways and to detect recruitment of the β-arrestins, enhanced bystander BRET (ebBRET) Effector Membrane Translocation Assay (EMTA) biosensors⁹ were used in HEK-293 cells. HEK-293 clonal cell lines were a gift from S. Laporte (McGill University, Montreal, Quebec, Canada). The plasmids p63-RhoGEF-RlucII, Rap1Gap-RlucII, β-arrestin1-RlucII, β-arrestin2-RlucII and rGFP-CAAX have been previously described^{52–54} and the human 5-HT_{2A}R was a gift from Domain Therapeutics North America. See Supp. information for more details.

Ligand binding studies

A total of 5-HT_{2A}R competition binding experiments were carried out in a polypropylene 96-well plate. In each well was incubated 70 μg of membranes from CHO-5-HT_{2A} cell line prepared in our laboratory (Lot: A006/10-03-2020, protein concentration=5134 μg/ml), 1 nM [³H]ketanserin (47.3 Ci/mmol, 1 mCi/ml, Perkin Elmer NET791250UC) and compounds studied and standard. Non-specific binding was determined in the presence of methysergide 1 μM (Sigma M137). The reaction mixture (Vt: 250 μl/well) was incubated at 37 °C for 30 min, 200 μl was transferred to GF/B 96-well plate (Millipore, Madrid, Spain) pretreated with 0.5% of PEI and treated with binding buffer (Tris-HCl 50 mM, pH=7.4), after was filtered and washed six times with 250 μl wash buffer (Tris-HCl 50 mM, pH=6.6), before measuring in a microplate beta scintillation counter (Microbeta Trilux, PerkinElmer, Madrid, Spain).

Brain prefrontal cortex membranes preparation

Human brain samples were obtained at autopsy in the Basque Institute of Legal Medicine, Bilbao, Spain, in compliance with policies of research

and ethical boards for postmortem brain studies at the moment of sample obtaining. Thus, samples from 12 different subjects (10 males and 2 females) with ages between 29–90 years were included. The postmortem delay between death and storage of the samples ranged from 4 to 12 h, and the storage time between sampling and experiments ranged from 48 to 10 months. All the subjects were determined to be free of neurological and psychiatric disorders based on medical records and postmortem tissue examinations. Positive blood toxicology for drugs or ethanol was considered exclusion criteria. Samples from the dorsolateral prefrontal cortex (PFC) were dissected at autopsy following established protocols³⁵ and immediately stored at -70°C until assay. Adult C57BL/6J mice were sacrificed by cervical dislocation, brains removed, PFC samples dissected, and samples stored at -70°C until assay. See Supp. Information for more details.

Antibody-capture [³⁵S]GTPγS binding scintillation proximity assay (SPA)

Specific activation of different subtypes of G proteins was determined using a homogeneous protocol of [³⁵S]GTPγS SPA coupled with the use of specific antibodies essentially as previously described^{16,17} following experimental conditions for determination of agonism, antagonism or inverse agonism properties of tested drugs. A single submaximal concentration of the drugs ($10\ \mu\text{M}$) was used. This submaximal concentration was chosen, as previously reported^{18,56,57}, as able to give us binding values around the maximal effect for any drug and subunit subtype combination studied. See Supplementary Information for more details on antibody specificities (Fig. S8).

Behavioral studies

Animals. We used male homozygous 5-HT_{2A}R KO mice and WT littermates on a C57BL/6J background (Charles River, France) (25–30 g). Since females have not been tested, this study does not address sex-related differences. 5-HT_{2A}R KO mice and WT littermates were bred in the animal facilities of the PRBB. Mice were initially grouped-housed in a room with controlled-temperature ($21 \pm 1^{\circ}\text{C}$) and humidity ($55 \pm 10\%$) environment with food and water available *ad libitum*. All the experiments were performed during the dark phase of the light/dark cycle (lights off at 8 a.m. and on at 8 p.m.), by observers blind to the experimental conditions.

Intracerebroventricular surgery and infusion. Nitro-I, Met-I, OTV1 and OTV2 and DOI were administered intracerebroventricularly (ICV). See Supp. Information for more details.

Behavioral Tests

Irwin test, head twitch response (HTR). Immediately following the ICV infusion, mice were placed in a transparent Plexiglas cylinder (30 cm in diameter and 50 cm high) and the Irwin test and HTR were quantified during 30 min. In a modified Irwin test⁵⁸ we evaluated behavioral dysfunction produced by 5-HT_{2A}R ligands and to estimate the minimum lethal dose and the range dose of each compound (data not shown). Some symptoms were evaluated by their presence or absence (lethality, convulsions, straub tail, abnormal gait, jumps, motor incoordination, piloerection, tremor, excitation, low reactivity to touch, and akinesia). Other symptoms, such as stereotypic behaviors (grooming, rearing, and scratching), were measured by the sum of events that occurred in 30 min. The HTR, characterized by a rapid side-to-side rotational head movement, was measured during 30 min following drug administration⁵⁹.

The novel object recognition (NOR) test. This test was performed to evaluate long-term memory deficits, as previously described¹⁹. The test consists of a black Plexiglas “V” maze with two corridors (30 cm long x 4.5 cm wide, and 15 cm high walls) set at a 90° angle (Panlab, Barcelona, Spain). See Supp. Information for more details.

Sucrose preference test. The sucrose preference test was used to evaluate negative symptoms associated with schizophrenia, such as anhedonia⁶⁰. See Supp. Information for more details.

Experimental procedures. To examine the dose-related effects of the compounds on HTR, different doses of pharmacological probes (0.025, 0.05, 0.1 and $0.5\ \mu\text{g}/\mu\text{l}$) or vehicle (VEH) were administered to C57BL/6J. A set of mice received all doses of OTV1, and OTV2 and VEH ($n = 5\text{--}11$). Another set of mice received all doses of Nitro-I and VEH ($n = 6\text{--}11$), and an additional set of mice received all doses of Met-I (0.025, 0.05, 0.1, and $0.5\ \mu\text{g}/\mu\text{l}$) and VEH ($n = 5\text{--}12$) in a Latin square design with a 3-day wash-out period between ICV infusions. Immediately after ICV infusions, mice were placed in a transparent Plexiglas cylinder and HTR were quantified during 30 min.

To evaluate the role of 5-HT_{2A}R on the behavioral responses to the different compounds, WT ($n = 5$) and 5-HT_{2A}R KO ($n = 6$) mice received OTV1, OTV2, Nitro-I, Met-I ($0.025, 0.05\ \mu\text{g}/\mu\text{l}$) and VEH in a Latin square design with a 3-day wash-out period between ICV infusions. Mice were first habituated (day 1) and then trained (day 2) in the NOR apparatus. Immediately after training, mice received ICV infusions and were placed in a transparent Plexiglas cylinder for 30 min to evaluate the Irwin test and HTR. 24 h after the ICV infusion, mice were tested in the NOR apparatus. Following a 3-day wash-out period, mice were habituated to the sucrose preference test for 3 days. On the fourth day, mice again received ICV infusions, and were presented with two volumetric pipettes, one containing drinking water and the other containing 1% sucrose. The intake of water and sucrose was measured daily every 24 h during 3 days.

To evaluate the role of G_{αq/11} on HTR and long-term memory deficits induced by OTV2 ($0.025, 0.05\ \mu\text{g}/\mu\text{l}$), two separate Latin square designs were implemented in naive C57BL/6J mice. Mice were habituated (day 1) and trained (day 2) to the NOR apparatus. Immediately after training, they received an ICV infusion of a vehicle solution, and 220 min later, ICV infusions of OTV2 were performed and HTR was measured. The following day, the NOR test was performed. Another group ($n = 5$) followed the same procedure but instead first received one ICV infusion of the G_{αq/11} inhibitor YM-254890 ($16\ \mu\text{M}$), and 220 min later, ICV infusions of OTV2 were performed (Fig. S7A).

To evaluate the role of G_{αi1} and G_{αi3} on the effects of OTV2, four sets of C57BL/6J mice ($n = 5/\text{group}$) were tested according to a Latin square design with a 3-day wash-out period in between infusions. One set received ICV infusions of either ODN, ODN-RD or distilled water as vehicle using the following schedule: on days 1 and 2 mice received 1 nmol, on days 3 and 4 they received 2 nmols, and on day 5 they received 3 nmols, as previously described⁶¹. On day 5 (before the ICV infusions), mice were habituated in the NOR. On day 6, mice were first trained in the NOR and then received ICV infusions of OTV2, and the HTR was measured for 30 min. On day 7, the NOR test was performed (Fig. S7B).

Western blots

To test whether G_{αi1} and G_{αi3} protein levels were significantly decreased by specific ODNs, Western blot analysis was carried out (see Supp. Information for more details).

Structural models for molecular dynamics simulations

The receptor was modeled based on PDB ID 6WHA, which is an active structure bound to an agonist, 25CN-NBOH, and coupled to miniG_q. To curate the structure, thermostabilizing and homogenizing alanine mutations at L247 and L371 were reverted. The missing parts of the structure (the beginning of the TM1, extracellular loops and missing side chains) were modeled using MODELLER⁶². Of note, multiple structures (PDB ID 6A93 and PDB ID 6A94 structures) were used as templates for modeling the extracellular loop. The four small molecules, including Nitro-I, Met-I, as well as the newly retrieved OTV1 and

OTV2, were docked to the receptor using the Molecular Operating Environment (MOE) with the triangle matcher as the placement method. The program was set to generate 30 poses for each molecule. The top 5 remaining after visual inspection were subjected to energy minimization using the MMFF94x force field while keeping the receptor rigid. The resulting poses were further analyzed, with special attention to the interaction with D3.32, as this is necessary for the activation of the aminergic receptors.

Molecular dynamics simulations and conformational clustering

In a next step, systems of the obtained ligand-5-HT_{2A}R complexes embedded in a hydrated membrane bilayer were generated. For this, internal waters were introduced into the receptor using Homolwat⁶³, and the protonation states of protein residues were decided using ProteinPrepare from the python module HTMD⁶⁴. In a next step, the ligand receptor complexes were embedded in a lipidic POPC bilayer, solvated with TIP3 waters and ionized with 150 mM Na⁺ or Cl⁻ ions. Models were equilibrated using ACEMD3⁶⁵ in NPT conditions for 40 ns. To ensure sufficient sampling of ligand-receptor contacts, each system was simulated for 3 × 500 ns (1.5 μs per system) in NVT conditions using ACEMD3 according to the state-of-the-art³⁴. Non-bonded interactions were cut-off at 9 Å. A smooth switching function for the cut-off was applied, starting at 7.5 Å. Long-distance electrostatic forces were calculated using the Particle Mesh Ewald algorithm. All simulations were carried out at a temperature of 310 K using the Langevin thermostat with damping constants γ of 1 ps⁻¹ and 0.1 ps⁻¹ for NPT and NVT simulations, respectively.

The trajectories obtained from the three replicates were concatenated into one trajectory file and clustered based on the movements of ligands using the average linkage analysis in CPPTRAJ⁶⁶. The cut off for the RMSD of the ligand for clustering was set to 5 Å. The contact and binding mode analysis were performed on the main cluster of each system. Receptor-ligand contacts were investigated in the GPCRmd workbench (www.gpcrmd.org). Contacts within 3 Å of the ligand which occurred with a frequency above 50% in the main cluster of the MD simulations were investigated.

The simulation data are made available via the GPCRmd repository (www.gpcrmd.org)³⁴:

Met-I bound to 5-HT_{2A}R: <https://submission.gpcrmd.org/view/1105/>

Nitro-I bound to 5-HT_{2A}R: <https://submission.gpcrmd.org/view/1107/>

OTV1 bound to 5-HT_{2A}R: <https://submission.gpcrmd.org/view/1128/>

OTV2 bound to 5-HT_{2A}R: <https://submission.gpcrmd.org/view/1110/>

LSD bound to 5-HT_{2A}R (PDB 6WGT): <https://submission.gpcrmd.org/view/1175/>

Lisuride bound to 5-HT_{2A}R (PDB 7WC7): <https://submission.gpcrmd.org/view/1176/>

Statistical analysis

In dose-response studies, one-way ANOVA were used to analyze the behavioral data comparing the different doses of Nitro-I, Met-I, OTV1 or OTV2. An unpaired Student's t test was used to analyze the data for DOI versus VEH administration. In studies evaluating the role of 5-HT_{2A}R, two-way ANOVAs were used to analyze the behavioral data with genotype (WT and 5-HT_{2A}R KO mice) as a between subject factor, and treatment (different doses of Nitro-I, Met-I, OTV1 or OTV2 and VEH) as a within subject factor. For G-protein studies, two-way ANOVAs were used to analyze the behavioral data with G-protein inhibitors (YM-254890, G_{αi1}-ODN, G_{αi3}-ODN, ODN-RD and VEH) as a between subject factor, and treatment (different doses of OTV2 and VEH) as a within subject factor. Fisher's LSD *post-hoc* tests for multiple comparisons were performed when appropriate. Specific [³⁵S]GTPγS binding results were analyzed by one- and two-sample Student's t-test *vs* basal values (expressed as 100%) or between experimental groups, respectively. For Western blot assay,

statistical analysis for comparison of the means between random and specific ODN treatments was performed by a one-way ANOVA followed by *post hoc* Bonferroni for multiple comparisons. The statistical analyzes were performed with the "Statistica" programme, version 6 (StatSoft Inc.) and GraphPad Prism™. All data are presented as mean ± SEM and statistical significance was set at p < 0.05 level. The statistical values obtained for all behavioral studies are shown in Table S3.

Reporting summary

Further information on research design is available in the Nature Portfolio Reporting Summary linked to this article.

Data availability

Data supporting the findings of this manuscript are available as a Supplementary Information file. MD simulations are deposited at the GPCRmd database (www.gpcrmd.org). Met-I bound to 5-HT_{2A}R: [<https://submission.gpcrmd.org/view/1105/>]. Nitro-I bound to 5-HT_{2A}R: [<https://submission.gpcrmd.org/view/1107/>]. OTV1 bound to 5-HT_{2A}R: [<https://submission.gpcrmd.org/view/1128/>]. OTV2 bound to 5-HT_{2A}R: [<https://submission.gpcrmd.org/view/1110/>]. LSD bound to 5-HT_{2A}R (PDB 6WGT): [<https://submission.gpcrmd.org/view/1175/>]. Lisuride bound to 5-HT_{2A}R (PDB 7WC7): [<https://submission.gpcrmd.org/view/1176/>]. Additional data supporting the findings are available from the corresponding authors upon request. A Source Data file is included with this manuscript. Source data are provided with this paper.

References

- Hauser, A. S., Attwood, M. M., Rask-Andersen, M., Schiöth, H. B. & Gloriam, D. E. Trends in GPCR drug discovery: new agents, targets and indications. *Nat. Rev. Drug Discov.* **16**, 829–842 (2017).
- Kenakin, T. Signaling bias in drug discovery. *Expert Opin. Drug Discov.* **12**, 321–333 (2017).
- Martí-Solano, M. et al. Detection of new biased agonists for the serotonin 5-HT_{2A} receptor: modeling and experimental validation. *Mol. Pharmacol.* **87**, 740–746 (2015).
- Kendler, K. S. Phenomenology of schizophrenia and the representativeness of modern diagnostic criteria. *JAMA Psychiatry* **73**, 1082–1092 (2016).
- Giuliani, L. et al. Improving Knowledge on Pathways to Functional Outcome in Schizophrenia: Main Results From the Italian Network for Research on Psychoses. *Front. Psychiatry* **12**, 791117 (2021).
- Elkis, H. & Buckley, P. F. Treatment-Resistant Schizophrenia. *Psychiatr. Clin. North Am.* **39**, 239–265 (2016).
- Kolb, P. et al. Community guidelines for GPCR ligand bias: IUPHAR review 32. *Br. J. Pharmacol.* **179**, 3651–3674 (2022).
- Kurita, M. et al. HDAC2 regulates atypical antipsychotic responses through the modulation of mGlu2 promoter activity. *Nat. Neurosci.* **15**, 1245–1254 (2012).
- González-Maeso, J. et al. Hallucinogens recruit specific cortical 5-HT(2A) receptor-mediated signaling pathways to affect behavior. *Neuron* **53**, 439–452 (2007).
- Kurrasch-Orbaugh, D. M., Watts, V. J., Barker, E. L. & Nichols, D. E. Serotonin 5-hydroxytryptamine 2A receptor-coupled phospholipase C and phospholipase A2 signaling pathways have different receptor reserves. *J. Pharmacol. Exp. Ther.* **304**, 229–237 (2003).
- Rodríguez, R. M. et al. LSD-stimulated behaviors in mice require β-arrestin 2 but not β-arrestin 1. *Sci. Rep.* **11**, 17690 (2021).
- Schmid, C. L., Raehal, K. M. & Bohn, L. M. Agonist-directed signaling of the serotonin 2A receptor depends on beta-arrestin-2 interactions in vivo. *Proc. Natl Acad. Sci. USA.* **105**, 1079–1084 (2008).
- Kenakin, T. & Christopoulos, A. Signaling bias in new drug discovery: detection, quantification and therapeutic impact. *Nat. Rev. Drug Discov.* **12**, 205–216 (2013).

14. Nagi, K. & Pineyro, G. Practical guide for calculating and representing biased signaling by GPCR ligands: A stepwise approach. *Methods* **92**, 78–86 (2016).
15. Piñeyro, G., Azzi, M., deLéan, A., Schiller, P. W. & Bouvier, M. Reciprocal regulation of agonist and inverse agonist signaling efficacy upon short-term treatment of the human delta-opioid receptor with an inverse agonist. *Mol. Pharmacol.* **67**, 336–348 (2005).
16. Diez-Alarcia, R. et al. Functional approaches to the study of G-protein-coupled receptors in postmortem brain tissue: [35S]GTPγS binding assays combined with immunoprecipitation. *Pharmacol. Rep.* **73**, 1079–1095 (2021).
17. Diez-Alarcia, R. et al. Biased Agonism of Three Different Cannabinoid Receptor Agonists in Mouse Brain Cortex. *Front. Pharmacol.* **7**, 415 (2016).
18. Muneta-Arrate, I., Diez-Alarcia, R., Horrillo, I. & Meana, J. J. Pimavanserin exhibits serotonin 5-HT_{2A} receptor inverse agonism for Gα_{i1}- and neutral antagonism for Gα_q/11-proteins in human brain cortex. *Eur. Neuropsychopharmacol.* **36**, 83–89 (2020).
19. Viñals, X. et al. Cognitive Impairment Induced by Delta9-tetrahydrocannabinol Occurs through Heteromers between Cannabinoid CB₁ and Serotonin 5-HT_{2A} Receptors. *PLoS Biol.* **13**, e1002194 (2015).
20. Corne, S. J. & Pickering, R. W. A possible correlation between drug-induced hallucinations in man and a behavioural response in mice. *Psychopharmacologia* **11**, 65–78 (1967).
21. González-Maeso, J. et al. Transcriptome fingerprints distinguish hallucinogenic and nonhallucinogenic 5-hydroxytryptamine 2A receptor agonist effects in mouse somatosensory cortex. *J. Neurosci.* **23**, 8836–8843 (2003).
22. Schmid, C. L. & Bohn, L. M. Serotonin, but not N-methyltryptamines, activates the serotonin 2A receptor via a β-arrestin2/Src/Akt signaling complex in vivo. *J. Neurosci.* **30**, 13513–13524 (2010).
23. Silva, M. T. & Calil, H. M. Screening hallucinogenic drugs: systematic study of three behavioral tests. *Psychopharmacologia* **42**, 163–171 (1975).
24. Tadano, T. et al. alpha-Methylated tryptamine derivatives induce a 5-HT receptor-mediated head-twitch response in mice. *Neuropharmacology* **34**, 229–234 (1995).
25. Wallach, J. et al. Identification of 5-HT_{2A} receptor signaling pathways associated with psychedelic potential. *Nat. Commun.* **14**, 8221 (2023).
26. Garzón, J., de Antonio, I. & Sánchez-Blázquez, P. In vivo modulation of G proteins and opioid receptor function by antisense oligodeoxynucleotides. *Methods Enzymol.* **314**, 3–20 (2000).
27. Garcia, E. E., Smith, R. L. & Sanders-Bush, E. Role of G(q) protein in behavioral effects of the hallucinogenic drug 1-(2,5-dimethoxy-4-iodophenyl)-2-aminopropane. *Neuropharmacology* **52**, 1671–1677 (2007).
28. Cunningham, M. J. et al. Pharmacological Mechanism of the Non-hallucinogenic 5-HT_{2A} Agonist Ariadne and Analogs. *ACS Chem. Neurosci.* **14**, 119–135 (2023).
29. Lewis, V. et al. A non-hallucinogenic LSD analog with therapeutic potential for mood disorders. *Cell Rep.* **42**, 112203 (2023).
30. Liu, X. et al. Gs signaling pathway distinguishes hallucinogenic and nonhallucinogenic 5-HT_{2A} agonists induced head twitch response in mice. *Biochem. Biophys. Res. Commun.* **598**, 20–25 (2022).
31. Zhu, H. et al. Gβγ subunit inhibitor decreases DOM-induced head twitch response via the PLCβ/IP3/Ca²⁺/ERK and cAMP signaling pathways. *Eur. J. Pharmacol.* **957**, 176038 (2023).
32. Torrens-Fontanals, M. et al. How do molecular dynamics data complement static structural data of GPCRs. *Int. J. Mol. Sci.* **21**, 5933 (2020).
33. Torrens-Fontanals, M., Stepniewski, T. M., Gloriam, D. E. & Selent, J. Structural dynamics bridge the gap between the genetic and functional levels of GPCRs. *Curr. Opin. Struct. Biol.* **69**, 150–159 (2021).
34. Rodríguez-Espigares, I. et al. GPCRmd uncovers the dynamics of the 3D-GPCRome. *Nat. Methods* **17**, 777–787 (2020).
35. Stepniewski, T. M. et al. Mechanistic insights into dopaminergic and serotonergic neurotransmission - concerted interactions with helices 5 and 6 drive the functional outcome. *Chem. Sci.* **12**, 10990–11003 (2021).
36. Duan, W., Cao, D., Wang, S. & Cheng, J. Serotonin 2A receptor (5-HT_{2A}R) agonists: psychedelics and non-hallucinogenic analogues as emerging antidepressants. *Chem. Rev.* **124**, 124–163 (2024).
37. Braden, M. R., Parrish, J. C., Naylor, J. C. & Nichols, D. E. Molecular interaction of serotonin 5-HT_{2A} receptor residues Phe339(6.51) and Phe340(6.52) with superpotent N-benzyl phenethylamine agonists. *Mol. Pharmacol.* **70**, 1956–1964 (2006).
38. Kimura, K. T. et al. Structures of the 5-HT_{2A} receptor in complex with the antipsychotics risperidone and zotepine. *Nat. Struct. Mol. Biol.* **26**, 121–128 (2019).
39. Kim, K. et al. Structure of a hallucinogen-activated Gq-coupled 5-HT_{2A} serotonin receptor. *Cell* **182**, 1574–1588.e19 (2020).
40. Wacker, D. et al. Crystal Structure of an LSD-Bound Human Serotonin Receptor. *Cell* **168**, 377–389.e12 (2017).
41. García-Bea, A. et al. Serotonin 5-HT_{2A} receptor expression and functionality in postmortem frontal cortex of subjects with schizophrenia: Selective biased agonism via Gα_{i1}-proteins. *Eur. Neuropsychopharmacol.* **29**, 1453–1463 (2019).
42. Ibarra-Lecue, I. et al. Chronic cannabis promotes pro-hallucinogenic signaling of 5-HT_{2A} receptors through Akt/mTOR pathway. *Neuropsychopharmacology* **43**, 2028–2035 (2018).
43. Karaki, S. et al. Quantitative phosphoproteomics unravels biased phosphorylation of serotonin 2A receptor at Ser280 by hallucinogenic versus nonhallucinogenic agonists. *Mol. Cell. Proteom.* **13**, 1273–1285 (2014).
44. Zhang, G. & Stackman, R. W. Jr. The role of serotonin 5-HT_{2A} receptors in memory and cognition. *Front. Pharmacol.* **6**, 225 (2015).
45. López-Giménez, J. F. & González-Maeso, J. Hallucinogens and Serotonin 5-HT_{2A} Receptor-Mediated Signaling Pathways. *Curr. Top. Behav. Neurosci.* **36**, 45–73 (2018).
46. Meneses, A. Stimulation of 5-HT_{1A}, 5-HT_{1B}, 5-HT_{2A/2C}, 5-HT₃ and 5-HT₄ receptors or 5-HT uptake inhibition: short- and long-term memory. *Behav. Brain Res.* **184**, 81–90 (2007).
47. MacKenzie, N. E. et al. Antipsychotics, metabolic adverse effects, and cognitive function in schizophrenia. *Front. Psychiatry* **9**, 622 (2018).
48. Sterling, T. & Irwin, J. J. ZINC 15–Ligand Discovery for Everyone. *J. Chem. Inf. Model.* **55**, 2324–2337 (2015).
49. Halgren, T. A. et al. Glide: a new approach for rapid, accurate docking and scoring. 2. Enrichment factors in database screening. *J. Med. Chem.* **47**, 1750–1759 (2004).
50. Knight, A. R. et al. Pharmacological characterisation of the agonist radioligand binding site of 5-HT_{2A}, 5-HT_{2B} and 5-HT_{2C} receptors. *Naunyn. Schmiedebergs. Arch. Pharmacol.* **370**, 114–123 (2004).
51. Pehek, E. A., Nocjar, C., Roth, B. L., Byrd, T. A. & Mabrouk, O. S. Evidence for the preferential involvement of 5-HT_{2A} serotonin receptors in stress- and drug-induced dopamine release in the rat medial prefrontal cortex. *Neuropsychopharmacology* **31**, 265–277 (2006).
52. Avet, C. et al. Effector membrane translocation biosensors reveal G protein and β-arrestin coupling profiles of 100 therapeutically relevant GPCRs. *Elife* **11**, e74101 (2022).
53. Namkung, Y. et al. Monitoring G protein-coupled receptor and β-arrestin trafficking in live cells using enhanced bystander BRET. *Nat. Commun.* **7**, 12178 (2016).
54. Namkung, Y. et al. Functional selectivity profiling of the angiotensin II type 1 receptor using pathway-wide BRET signaling sensors. *Sci. Signal.* **11**, eaat1631 (2018).

55. Muguruza, C. et al. Dysregulated 5-HT(2A) receptor binding in postmortem frontal cortex of schizophrenic subjects. *Eur. Neuropsychopharmacol.* **23**, 852–864 (2013).
56. Diez-Alarcia, R. et al. Big data challenges targeting proteins in gpcr signaling pathways; combining ptml-chembl models and [35s]gtpys binding assays. *ACS Chem. Neurosci.* **10**, 4476–4491 (2019).
57. Erdozain, A. M., Diez-Alarcia, R., Meana, J. J. & Callado, L. F. The inverse agonist effect of rimonabant on G protein activation is not mediated by the cannabinoid CB1 receptor: evidence from post-mortem human brain. *Biochem. Pharmacol.* **83**, 260–268 (2012).
58. Irwin, S. Comprehensive observational assessment: Ia. A systematic, quantitative procedure for assessing the behavioral and physiologic state of the mouse. *Psychopharmacologia* **13**, 222–257 (1968).
59. Halberstadt, A. L. & Geyer, M. A. Characterization of the head-twitch response induced by hallucinogens in mice: detection of the behavior based on the dynamics of head movement. *Psychopharmacology* **227**, 727–739 (2013).
60. He, L.-W. et al. Optimization of food deprivation and sucrose preference test in SD rat model undergoing chronic unpredictable mild stress. *Anim. Model Exp. Med.* **3**, 69–78 (2020).
61. Sánchez-Blázquez, P., Gómez-Serranillos, P. & Garzón, J. Agonists determine the pattern of G-protein activation in mu-opioid receptor-mediated supraspinal analgesia. *Brain Res. Bull.* **54**, 229–235 (2001).
62. Eswar, N. et al. Comparative protein structure modeling using Modeller. *Curr. Protoc. Bioinformatics Ch.* **5**, Unit-5.6 (2006).
63. Mayol, E. et al. HomolWat: a web server tool to incorporate ‘homologous’ water molecules into GPCR structures. *Nucleic Acids Res.* **48**, W54–W59 (2020).
64. Doerr, S., Harvey, M. J., Noé, F. & De Fabritiis, G. HTMD: High-Throughput Molecular Dynamics for Molecular Discovery. *J. Chem. Theory Comput.* **12**, 1845–1852 (2016).
65. Harvey, M. J., Giupponi, G. & Fabritiis, G. D. ACEMD: Accelerating Biomolecular Dynamics in the Microsecond Time Scale. *J. Chem. Theory Comput.* **5**, 1632–1639 (2009).
66. Roe, D. R. & Cheatham, T. E. PTRAJ and CPPTRAJ: Software for Processing and Analysis of Molecular Dynamics Trajectory Data. *J. Chem. Theory Comput.* **9**, 3084–3095 (2013). 3rd.

Acknowledgements

This work was supported by the ERANET NEURON consortium fund (funding was provided by CIHR NDD-161471 and FRQ-S 278647 for M.B., the German Federal Ministry of Education and Research under grant number O1EW1909 for P.K., as well as the Instituto de Salud Carlos III and Fondo Europeo de Desarrollo Regional number AC18/00030 for J.S. and P.R.). This work was further supported by the Instituto de Salud Carlos III (ISCIII) and co-funded by the European Union (PI18/00094) to J.S. and (PI18/00053) to P.R. We acknowledge grant support from Agencia Estatal de Investigación (PID2020-119428RB-I00; SAF2017-88126R), Basque Government (IT-1211/19, IT-1512/22 and KK-2019/00-49), Xunta de Galicia (ED431C 2022/20 and ED431G 2019/02) and European Regional Development Fund (ERDF). P.K. thanks the German Research Foundation DFG for Heisenberg Professorship KO4095/5-1. S.S.O. and R.S. thank the PTQ-17-09103 (Ayuda Torres Quevedo, Ministerio de Ciencia e Innovación), and BioExcel-2 (Grant Number 823830, Horizon2020). M.B. was in part supported by an operating grant (# PJT 183758) from the Canadian Institute for Health Research. I.M.-A. was the

recipient of a predoctoral fellowship from the Basque Government. The authors would like to thank the staff members of the Basque Institute of Legal Medicine for their cooperation in the study, especially to Dr. Benito Morentin. R.D.-A., T.M.S, D.A.G., I.M.A., A.S., P.K. and J.S. are members of COST Action CA18133 “ERNEST”.

Author contributions

P.R. and J.S. conceived and designed the study. E.K. and C.R.D. supervised by R.T. and P.R. performed the behavioral studies in mice. R.D.A., I.M.A., and J.J.M. carried out receptor coupling experiments in human and mice brain tissue. S.A.G. and E.T. supervised by MB conducted the cell-based BRET assays. A.S., D.A.G., and T.M.S. supervised by P.K. and J.S. built structural models and carried out molecular dynamics simulations. S.S.O. and R.S. performed the virtual screening. D.M., J.B., and M.I.L. conducted the ligand binding assays. P.R. and J.S. wrote the manuscript with main contributions from R.D.A., E.K. and M.B. All authors revised the manuscript. P.R. and J.S. supervised and coordinated the whole project.

Competing interests

The authors declare no competing interests.

Additional information

Supplementary information The online version contains supplementary material available at <https://doi.org/10.1038/s41467-024-48196-2>.

Correspondence and requests for materials should be addressed to Patricia Robledo or Jana Selent.

Peer review information *Nature Communications* thanks Javier González-Maeso and the other, anonymous, reviewer for their contribution to the peer review of this work. A peer review file is available.

Reprints and permissions information is available at <http://www.nature.com/reprints>

Publisher’s note Springer Nature remains neutral with regard to jurisdictional claims in published maps and institutional affiliations.

Open Access This article is licensed under a Creative Commons Attribution 4.0 International License, which permits use, sharing, adaptation, distribution and reproduction in any medium or format, as long as you give appropriate credit to the original author(s) and the source, provide a link to the Creative Commons licence, and indicate if changes were made. The images or other third party material in this article are included in the article’s Creative Commons licence, unless indicated otherwise in a credit line to the material. If material is not included in the article’s Creative Commons licence and your intended use is not permitted by statutory regulation or exceeds the permitted use, you will need to obtain permission directly from the copyright holder. To view a copy of this licence, visit <http://creativecommons.org/licenses/by/4.0/>.

© The Author(s) 2024

¹Integrative Pharmacology and Systems Neuroscience Research Group, Hospital del Mar Research Institute, Barcelona, Spain. ²Department of Pharmacology, University of the Basque Country/Euskal Herriko Unibertsitatea, Leioa, Bizkaia, Spain. ³Centro de Investigación Biomédica en Red de Salud Mental CIBERSAM, Madrid, Spain. ⁴Instituto de Investigación Sanitaria Biobizkaia, Barakaldo, Bizkaia, Spain. ⁵Department of Biochemistry and Molecular Medicine, Institute for Research in Immunology and Cancer (IRIC), Université de Montréal, Montréal, Québec H3T 1J4, Canada. ⁶Cell-type mechanisms in normal and pathological behaviour Research Group, IMIM-Hospital del Mar Medical Research Institute, Barcelona, Spain. ⁷Research Programme on Biomedical Informatics (GRIB),

Hospital del Mar Research Institute, Barcelona, Spain. ⁸InterAx Biotech AG, PARK InnovaARE, 5234 Villigen, Switzerland. ⁹Department of Medicine and Life Sciences, Pompeu Fabra University, Barcelona, Spain. ¹⁰NBD NOSTRUM BIODISCOVERY, Av. de Josep Tarradellas, 8-10, 3-2, 08029 Barcelona, Spain. ¹¹Pharmaceutical Chemistry, University of Marburg, Marbacher Weg 8, Marburg 35037, Germany. ¹²Innopharma Drug Screening and Pharmacogenomics Platform. BioFarma research group. Center for Research in Molecular Medicine and Chronic Diseases (CiMUS). Department of Pharmacology, Pharmacy and Pharmaceutical Technology, University of Santiago de Compostela, Santiago de Compostela, Spain. ¹³Health Research Institute of Santiago de Compostela (IDIS), University Hospital of Santiago de Compostela (SERGAS), Trav. Choupana s/n, 15706 Santiago de Compostela, Spain. ¹⁴These authors contributed equally: Elk Kossatz, Rebeca Diez-Alarcia. ✉e-mail: probledo@imim.es; jana.selent@upf.edu